NASA/TP-1999-209536

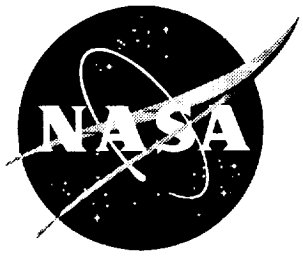

Design of Supersonic Transport Flap Systems for Thrust Recovery at Subsonic Speeds

Michael J. Mann
Langley Research Center, Hampton, Virginia

Harry W. Carlson and Christopher S. Domack
Lockheed Engineering & Sciences Company, Hampton, Virginia

December 1999

The NASA STI Program Office . . . in Profile

Since its founding, NASA has been dedicated to the advancement of aeronautics and space science. The NASA Scientific and Technical Information (STI) Program Office plays a key part in helping NASA maintain this important role.

The NASA STI Program Office is operated by Langley Research Center, the lead center for NASA's scientific and technical information. The NASA STI Program Office provides access to the NASA STI Database, the largest collection of aeronautical and space science STI in the world. The Program Office is also NASA's institutional mechanism for disseminating the results of its research and development activities. These results are published by NASA in the NASA STI Report Series, which includes the following report types:

- TECHNICAL PUBLICATION. Reports of completed research or a major significant phase of research that present the results of NASA programs and include extensive data or theoretical analysis. Includes compilations of significant scientific and technical data and information deemed to be of continuing reference value. NASA counterpart of peer-reviewed formal professional papers, but having less stringent limitations on manuscript length and extent of graphic presentations.

- TECHNICAL MEMORANDUM. Scientific and technical findings that are preliminary or of specialized interest, e.g., quick release reports, working papers, and bibliographies that contain minimal annotation. Does not contain extensive analysis.

- CONTRACTOR REPORT. Scientific and technical findings by NASA-sponsored contractors and grantees.

- CONFERENCE PUBLICATION. Collected papers from scientific and technical conferences, symposia, seminars, or other meetings sponsored or co-sponsored by NASA.

- SPECIAL PUBLICATION. Scientific, technical, or historical information from NASA programs, projects, and missions, often concerned with subjects having substantial public interest.

- TECHNICAL TRANSLATION. English-language translations of foreign scientific and technical material pertinent to NASA's mission.

Specialized services that complement the STI Program Office's diverse offerings include creating custom thesauri, building customized databases, organizing and publishing research results . . . even providing videos.

For more information about the NASA STI Program Office, see the following:

- Access the NASA STI Program Home Page at ***http://www.sti.nasa.gov***

- Email your question via the Internet to help@sti.nasa.gov

- Fax your question to the NASA STI Help Desk at (301) 621-0134

- Telephone the NASA STI Help Desk at (301) 621-0390

- Write to:
  NASA STI Help Desk
  NASA Center for AeroSpace Information
  7121 Standard Drive
  Hanover, MD 21076-1320

NASA/TP-1999-209536

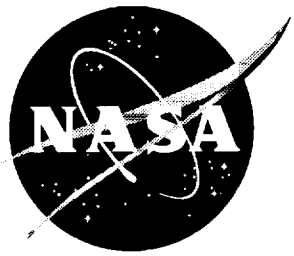

Design of Supersonic Transport Flap Systems for Thrust Recovery at Subsonic Speeds

Michael J. Mann
Langley Research Center, Hampton, Virginia

Harry W. Carlson and Christopher S. Domack
Lockheed Engineering & Sciences Company, Hampton, Virginia

National Aeronautics and
Space Administration

Langley Research Center
Hampton, Virginia 23681-2199

December 1999

Available from:

NASA Center for AeroSpace Information (CASI)
7121 Standard Drive
Hanover, MD 21076-1320
(301) 621-0390

National Technical Information Service (NTIS)
5285 Port Royal Road
Springfield, VA 22161-2171
(703) 605-6000

Abstract

A study of the subsonic aerodynamics of hinged flap systems for supersonic cruise commercial aircraft has been conducted using linear attached-flow theory that has been modified to include an estimate of attainable leading-edge thrust and an approximate representation of vortex forces. Comparisons of theoretical predictions with experimental results show that the theory gives a reasonably good and generally conservative estimate of the performance of an efficient flap system and provides a good estimate of the leading- and trailing-edge deflection angles necessary for optimum performance. A substantial reduction in the area of the inboard region of the leading-edge flap has only a minor effect on the performance and the optimum deflection angles. Changes in the size of the outboard leading-edge flap show that performance is greatest when this flap has a chord equal to approximately 30 percent of the wing chord. A study was also made of the performance of various combinations of individual leading- and trailing-edge flaps, and the results show that aerodynamic efficiencies as high as 85 percent of full suction are predicted.

Introduction

Several studies have been conducted to investigate the applicability of linear attached-flow theory to the design and analysis of subsonic flap systems for supersonic cruise vehicles (refs. 1 to 3). The linear theory methods utilized in these studies were modified to include an estimate of the attainable leading-edge thrust and the vortex forces that arise because of leading-edge flow separation. Extensive correlation with experimental results demonstrated that these modified linear methods provide a convenient and effective means for the preliminary design of flap systems that maximize aerodynamic performance in the subsonic speed range (below drag-divergence Mach number). At the design condition, the flow tends to be predominately attached. Therefore, the theory gives a good prediction of the aerodynamic performance at the design condition and provides a method for the identification of promising concepts for wind tunnel investigation.

The current theoretical study examines the design of an effective flap system for a supersonic transport. The requirement for efficient supersonic cruise performance results in highly swept, low-aspect-ratio thin wings twisted and cambered for maximum lift-drag ratio (L/D) at low lift coefficients. The modified linear theory methods of references 1 to 3 were used to devise leading- and trailing-edge flap systems that maximize aerodynamic performance at the subsonic speeds and higher lift coefficients necessary for takeoff and landing.

The discussion begins with a consideration of some fundamental characteristics of the flow over thin wings with and without deflected flaps. Several correlations between theory and experiment are used to illustrate the applicability of the modified linear theory to the prediction of subsonic flap performance. A detailed example of the theoretical flap design and analysis process is then given for a baseline flap system on a representative supersonic transport configuration. Finally, the theory is used to study the effects of changes in flap geometry on aerodynamic performance. This type of study provides the necessary information for design studies that balance the aerodynamic benefits of flap systems against their complexity, size, and weight.

Symbols

AR	aspect ratio, b^2/S
b	span, in.
C_D	drag coefficient
ΔC_D	drag coefficient due to lift, $C_D - C_{D,0}$
$C_{D,0}$	drag coefficient at $\alpha = 0°$ for wing with no camber, twist, or flap deflections
C_L	lift coefficient
$C_{L,\text{des}}$	design lift coefficient
C_{L_α}	theoretical lift-curve slope of flat wing near $\alpha = 0°$ with no leading-edge thrust or vortex force, per deg

C_m	pitching-moment coefficient
$C_{m,\text{des}}$	design pitching-moment coefficient
ΔC_p	lifting pressure coefficient
c	local chord, in.
$c_{f,\text{le}}$	streamwise leading-edge flap chord, in.
$c_{f,\text{le},o}$	streamwise leading-edge flap chord on outboard wing panel ($y \geq 18$ in.), in.
$c_{f,\text{le,sf}}$	streamwise leading-edge flap chord at side of fuselage ($y = 2.3$ in.), in.
$c_{f,\text{te}}$	streamwise trailing-edge flap chord, in.
c_r	chord of planform used in WINGDES2 and AERO2S codes at $y = 0$, in.
c_t	section leading-edge thrust coefficient
$c_{t,a}$	attainable thrust value of section leading-edge thrust coefficient
$c_{t,t}$	full theoretical value of section leading-edge thrust coefficient
L/D	lift-drag ratio
M	Mach number
$N_{c,\text{le}}$	number of computational elements on leading-edge flap
R	Reynolds number based on mean aerodynamic chord
r_{le}	leading-edge radius, in.
S	reference area, in^2
S_s	suction parameter, $\dfrac{C_L \tan(C_L/C_{L_\alpha}) - \Delta C_D}{C_L \tan(C_L/C_{L_\alpha}) - C_L^2/(\pi \text{AR})}$
t	section thickness, in.
x, y, z	Cartesian coordinates measured aft from nose, starboard from centerline, and up from leading edge, respectively, in.
x'	distance in x-direction measured from leading edge, in.
Δz	increment in z at leading or trailing edge, in.
α	angle of attack, deg
α_{des}	angle of attack corresponding to design lift coefficient, deg
α_{zt}	angle of attack for zero leading-edge thrust, deg
$\Delta\alpha_{\text{ft}}$	range of angle of attack for full leading-edge thrust, deg
δ_{le}	streamwise deflection angle of leading-edge flap, positive with leading edge down, deg
$\delta_{\text{le},n}$	leading-edge flap-deflection angle measured normal to hinge line, positive with leading edge down, deg
$\delta_{\text{le},r}$	leading-edge flap-deflection ratio equal to angle input to AERO2S code divided by nominal design value of streamwise deflection angle
δ_{te}	streamwise deflection angle of trailing-edge flap, positive with trailing edge down, deg
$\delta_{\text{te},n}$	trailing-edge flap-deflection angle measured normal to hinge line, positive with trailing edge down, deg
$\delta_{\text{te},r}$	trailing-edge flap-deflection ratio equal to angle input to AERO2S code divided by nominal design value of streamwise deflection angle
η	nondimensional semispan location, $y/(b/2)$

Subscripts:

des	design
le	leading edge
max	maximum
o	outboard wing panel
r	ratio
sf	side of fuselage
te	trailing edge

Configuration nomenclature:

L1, L2, L3	leading-edge flaps (see table B1)
T1, T2	trailing-edge flaps (see table B1)

Theoretical Considerations

Fundamental Aerodynamics of Flaps

Figure 1, which illustrates some fundamental characteristics of subsonic flow on wings with and without deflected flaps, compares the theoretical flow predicted by linear attached-flow methods with the real separated flow for several sharp leading-edge wing airfoil sections. The uncambered wing section on the left can be used to illustrate the behavior of a flat or mildly cambered supersonic wing with zero flap deflections. The theoretical lifting pressure

distribution on this wing has a very high peak at the leading edge that results in a theoretical leading-edge thrust counteracting much of the drag force over the rest of the wing. This thrust is predicted by the linear theory, even in the case of zero leading-edge thickness. (A leading-edge singularity occurs in the solution for this case.) A high level of aerodynamic efficiency could be achieved with this wing shape if the attached flow could be maintained at lifting conditions. However, as shown in the lower part of figure 1, the strong adverse pressure gradient at the leading edge causes the flow to separate, the result being an almost complete loss of the leading-edge thrust. With some finite leading-edge radius, the loss of thrust will be diminished. The undeveloped leading-edge thrust may be converted into a normal force according to the Polhamus suction analogy (ref. 4); however, the resulting flow has a substantially lower aerodynamic efficiency than an attached flow.

When a leading-edge flap is deflected, as shown in the next sketch in figure 1, the theoretical leading-edge suction peak is reduced and a second peak in lifting pressure distribution occurs at the flap hinge line. The wing now has a distributed thrust force produced by the lifting pressure acting on the forward projected area of the flap. The real flow can be kept predominately attached when flap-deflection angles are selected with design and analysis methods that employ the attainable leading-edge thrust theory of reference 5. The combination of distributed thrust and leading-edge thrust produces theoretical attached-flow performance that is comparable to that of the flat (uncambered) wing with full theoretical leading-edge thrust.

Deflection of the trailing-edge flap further improves the lifting efficiency by lowering the angle of attack required to produce the design lift. The lower angle of attack reduces the effects of separation at the leading edge and generally produces an aerodynamic flow that has less drag at the design lift coefficient.

The sketches at the far right in figure 1 show a wing that has been smoothly cambered to produce a minimum drag at the design lift. Because this surface maximizes the attached flow and efficient lift generation, it can be used as a guide for the selection of flap chords and flap deflections that approach those goals.

Theoretical Methods

The design method of the present study is based on the concept that a high level of aerodynamic efficiency results from a flow that is as nearly attached as possible (ref. 2). Flap deflections for simple hinged or plain flaps were, therefore, derived from smooth, optimized camber distributions designed for restricted areas of the wing at the leading and trailing edges. These optimum camber shapes were defined with the WINGDES2 linear theory design code (refs. 2 and 6). The method used by this code defines the mildest camber surface that will produce optimum performance (minimum axial force) at specified values of the lift and pitching moment. In order to prevent flow separation at the leading edge, the local incidence of the leading edge is determined by a design process that accounts for the attainable leading-edge thrust as described in reference 5. This method defines limitations on the leading-edge thrust as a function of wing geometry, Mach number, and Reynolds number. The camber in the leading-edge region develops a distributed thrust that effectively recovers the portion of the theoretical flat-wing leading-edge thrust that cannot be developed because of flow separation. The combination of the attainable leading-edge thrust and the distributed thrust produces performance comparable to that of a flat wing with full theoretical leading-edge thrust.

The theoretical smooth camber surfaces are designed for attached flow. The actual sharp leading-edge wing with simple hinged or plain flaps deflected to angles chosen to approximate the smooth camber design cannot produce a completely attached flow. However, any flow separation that does occur on the wing with flaps is likely to be mild and localized, as depicted in the real-flow sketches of figure 1.

The AERO2S code of reference 3 was used in the present study to estimate the aerodynamic performance of the wing with deflected flaps. This code is also based on linear theory. The theoretical results are also modified to include attainable leading-edge thrust and an estimate of the forces due to vortices produced by leading-edge flow separation. The code was developed to predict the effects of leading- and trailing-edge flaps on an isolated wing or on a wing in combination with a horizontal tail or canard. The theory accounts for the flap hinge-line singularity in a manner similar to that used for the leading-edge singularity.

Some comparisons between predictions of the AERO2S code and experimental results are shown in figures 2 and 3. The suction parameter used in these figures, which is employed throughout this paper as a measure of performance, is defined as

$$S_s = \frac{C_L \tan(C_L/C_{L_\alpha}) - \Delta C_D}{C_L \tan(C_L/C_{L_\alpha}) - C_L^2/(\pi \mathrm{AR})}$$

This parameter compares the drag of the configuration with upper and lower bounds. The upper bound, $C_{D,0} + C_L \tan(C_L/C_{L_\alpha})$, is the drag of a flat wing with no leading-edge thrust and no vortex force. The lower bound, $C_{D,0} + C_L^2/(\pi \mathrm{AR})$, is the theoretical drag of a wing with an elliptical spanwise load distribution and full leading-edge thrust. These limits correspond to the values of suction parameter of 0 and 1.0, respectively.

Figure 2 compares theoretical and experimental results for a supersonic cranked-wing fighter (ref. 7). The wing leading edge is swept 70° on the inboard section and 20° on the outboard section. The experimental study examined a large matrix of leading- and trailing-edge flap deflections. These data permitted the construction of the experimental performance contour map in figure 2, which shows lines of constant suction parameter as a function of leading- and trailing-edge flap deflections. Lines of constant pitching-moment coefficient and angle of attack are also shown. The experimental contour map is compared in figure 2 with a theoretical contour map constructed with the AERO2S code. The contour maps are presented for a lift coefficient of 0.45, a Mach number of 0.50, and a Reynolds number of 2.9×10^6. The maps can be used to determine the theoretical and experimental maximum suction parameters and the flap deflections necessary to produce the maximum suction parameter. The theoretical value of maximum suction parameter is 0.90, which agrees well with the experimental value of 0.89. The theory predicts flap-deflection angles for the peak suction parameter within about ±2° of the experimental values. The theory also gives a reasonably good estimate of the pitching moment and angle of attack for flap deflections in the vicinity of the peak suction parameter.

Figure 3 compares AERO2S predictions with experimental results for an arrow-wing supersonic transport (ref. 8). This configuration is more closely related to that of the present study than the fighter configuration of figure 2; however, the available experimental data are not as extensive. The wing of this configuration was twisted and cambered for supersonic cruise. The results of figure 3 are for a lift coefficient of 0.45, a Mach number of 0.21, and a Reynolds number of 4.1×10^6. The wing was tested with two different tapered leading-edge flaps and a segmented trailing-edge flap as shown.[1] Sufficient combinations of flap deflections were not tested to permit construction of an experimental performance contour plot. However, theoretical contour plots were developed for each flap geometry. The variables $\delta_{\mathrm{le},r}$ and $\delta_{\mathrm{te},r}$ are multipliers on the corresponding spanwise deflection schedules in figure 3. The solid symbols on the contour plots indicate experimental flap-deflection combinations that are compared with the theory in the adjacent bar graphs. The results show that the theory gives a reasonably good prediction of the suction parameter. In every case the theoretical estimate is conservative.

The twist and camber of a supersonic transport-wing is designed for the supersonic cruise condition and is, therefore, mild compared with the twist and camber needed for the low-speed and high-lift conditions of takeoff and landing. Although the supersonic twist and camber do provide some benefit at subsonic speeds, a low-speed flap study can be simplified by the use of a flat wing, especially if experimental studies are involved. The configuration in figure 3(a) was used to assess the effect of the supersonic cruise camber and twist on the maximum suction parameter and the required flap deflections for maximum suction for the flight conditions of figure 3. Figure 4 compares the theoretical performance contour plot for the twisted and cambered wing from figure 3(a) with the theoretical contour plot for a flat wing with the same flap geometry. These contour plots show that the flat wing develops only a slightly smaller maximum suction parameter (0.785 instead of 0.810) and has optimum leading- and trailing-edge flap deflections of 22° and 15°, respectively, compared with 19° and 13° for the cambered and twisted wing. Thus, for this configuration, the mild supersonic cruise twist and camber have only a relatively small effect on the maximum suction parameter and the optimum flap deflections. Because the results of the current theoretical study are to be experimentally examined in a future study using an existing flat or uncambered wing, the configuration for the current study (described in the next section) is assumed to have an uncambered wing and uncambered flaps.

Flap-System Design

Configuration Description

The configuration used in the present study is shown in figure 5. The geometric characteristics of the wing planform and airfoil sections are given in tables I to III. The variation of the leading-edge radius ratio (r_{le}/c) with thickness ratio $((t/c)_{\max})$ corresponds approximately with that of the NACA-64A-series airfoil sections (ref. 9). The fuselage is represented in the theory as part of the lifting surface

[1] The flap-deflection angles used in the current report are measured streamwise. The streamwise deflections for the flap with the moderate inboard leading-edge chord produce a constant normal deflection of 30° across the entire span.

by alteration of both the wing planform and the mean camber.

The wing area available for flap design is shown by the shaded areas in figure 5(a). A representative trailing-edge flap arrangement has been assumed. Because the twist and camber between the leading- and trailing-edge flaps remain unchanged during the design process, the resultant wing shape is called a restricted-area design. As discussed in the last section, the initial wing geometry was assumed to be uncambered (flat). Thus, the wing area remained uncambered outside of the design regions. The supersonic cruise twist and camber which would be present in an actual design would develop a small amount of distributed thrust at subsonic speeds (e.g., fig. 28 in ref. 3). The beneficial effect of this distributed thrust was seen in the example in figure 4 in which the maximum suction parameter was slightly higher and the flap-deflection angles were somewhat smaller for the cambered and twisted wing.

Some guidance in the selection of the spanwise distribution of leading-edge flap chord can be gained from the spanwise distribution of leading-edge thrust. Sketch A shows the spanwise variation of theoretical and attainable section leading-edge thrust coefficients on a flat wing for a lift coefficient of 0.45 and a Mach number of 0.20. The theoretical thrust builds up rapidly in the spanwise direction because of the increased upwash on the outboard sections. However, the attainable thrust curve shows that only a small portion of this theoretical concentrated leading-edge thrust can actually be developed. With the trailing-edge flaps deflected as shown in sketch B, a considerable difference still exists between the theoretical and attainable thrust. This difference between the flat-wing theoretical and attainable leading-edge thrust curves indicates a potential for the recovery of the unattained portion of the theoretical leading-edge thrust by the development of a distributed thrust on a leading-edge camber surface or a leading-edge flap. The flap chord required to support this distributed thrust tends to be proportional to the difference between the curves and is, therefore, small inboard and grows in size in the spanwise direction.

Based on the foregoing observations, the series of leading-edge flaps shown in figure 5(b) was selected for study. The taper of the inboard leading-edge flap was varied by the selection of three flap root chords ranging from 0 to 16 percent of the wing chord. The size of the outboard leading-edge flap was varied from 20 to 40 percent of wing chord. The area of the trailing-edge flaps remained fixed throughout the study. The geometry of the leading- and trailing-edge flaps shown in figure 5(b) is defined in table IV.

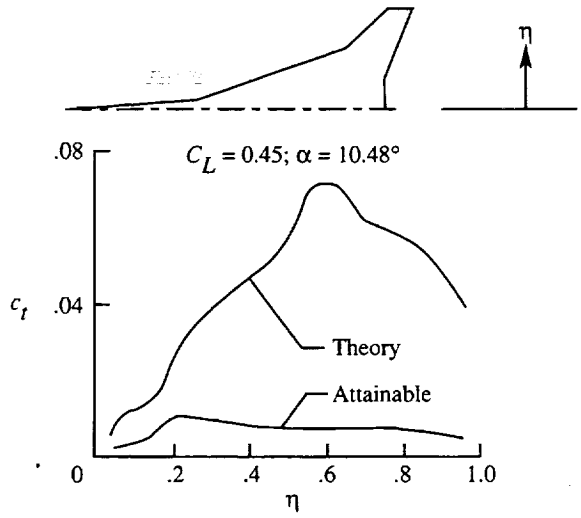

Sketch A

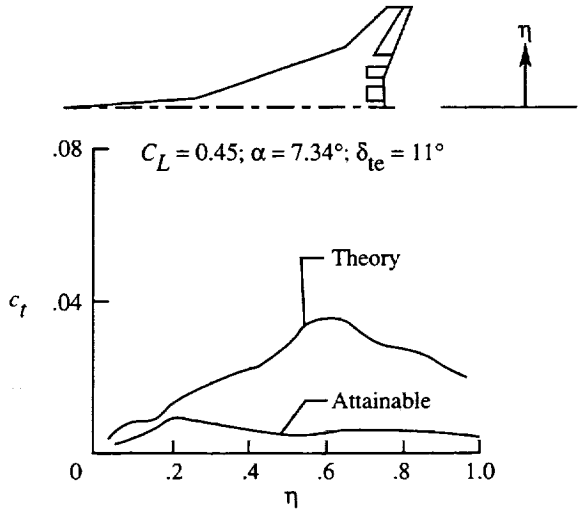

Sketch B

Design Conditions

The flap configurations treated in this study were designed for a 0.0326-scale model at a lift coefficient of 0.45, a Mach number of 0.20, and a wind tunnel Reynolds number of 5.38×10^6. The results of this study can be extended, within reasonable limits, to other conditions. The Mach number has a minor effect on the results up to the drag-divergence Mach number. Sketch C shows the variation of suction parameter with design lift coefficient for a representative flap design. The sketch illustrates that the flap-system performance has only a slight decrease at higher lift coefficients (provided that the

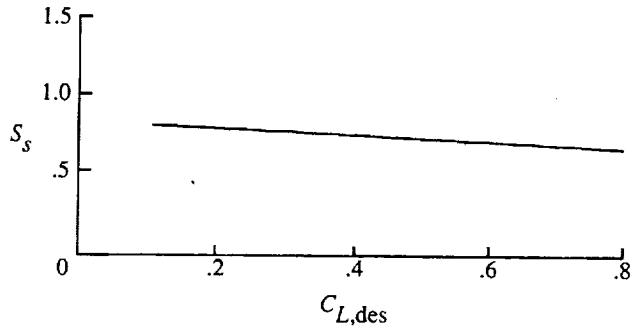

Sketch C

deflection angles are increased in accordance with theoretical estimates). The suction parameter has almost a linear dependence on $C_{L,\text{des}}$.

Although the current study does not involve a longitudinal trim requirement, the use of the WINGDES2 code for a restricted-area design without an appropriate constraint on pitching moment results in a design that underemphasizes trailing-edge camber or flaps. Some additional trailing-edge camber reduces the required leading- edge camber and thereby alleviates drag penalties associated with leading-edge camber that are not fully accounted for by the linear theory. The present study uses a procedure from references 2 and 10 that involves the use of a pitching-moment constraint to provide the additional trailing-edge camber. The value of the pitching-moment constraint is obtained from a design that utilizes the entire wing area and has no constraint on pitching moment. This is called a whole-wing design. The value of pitching moment at the design lift coefficient for this solution was used as the pitching-moment constraint for the restricted-area design. For the design conditions of the present study, the WINGDES2 code gave a pitching-moment constraint (design pitching moment) of -0.03. If trim conditions had been taken into account, the restricted-area design would be performed with the specified pitching-moment constraint rather than with the one derived from the whole-wing design.

This choice of design pitching-moment coefficient is further examined in figure 6 for the baseline flap system. Figure 6 shows the effect of pitching-moment constraint on the suction parameter and the trailing-edge flap deflection at $\eta = 0.75$. The baseline flap system has an inboard leading-edge flap that tapers to zero chord at the side of the fuselage and an outboard leading-edge flap that is 30 percent of the chord. The trailing-edge flap is also included in the baseline system. Optimum performance does indeed occur for a design pitching-moment coefficient of -0.03. At the optimum condition, the suction parameter is 0.925 and the trailing-edge flap deflection is 10°. Note, however, that when the code is employed without any constraint on pitching moment (unrestrained design), the resultant design has a lower suction parameter and a smaller trailing-edge flap deflection than the optimum design. (The leading-edge flap deflection, which is slightly larger than optimum, is not shown.) The problem is not significant for a whole-wing design, but it does occur for the restricted-area design in which relatively large surface slopes are needed to generate the required loadings on restricted areas. The code develops the proper amount of leading-edge camber for thrust recovery according to the attainable thrust methods; however, the optimization does not call for enough trailing-edge slope to get a true minimum drag.

Tables V(a) and V(b) give examples of input data for the WINGDES2 code for the whole-wing design and the restricted-area design, respectively. Descriptions of the code input and output are given in the appendixes of references 3 and 10. The weighting factors for the leading-edge modification surfaces (TAFIX), which provide a smoothing of numerical solution surface irregularities and may improve aerodynamic performance, are suggested values from prior runs in which no TAFIX were input.

Flap-Design Process

The flap-design process is now described in detail for the baseline case. As discussed earlier, the WINGDES2 code is first used to design optimum camber surfaces in leading- and trailing-edge areas that include the flaps, as shown by the upper sketch in figure 7. The wing camber between the crosshatched areas remains unchanged during the design process for this restricted-area design. The chords of these design areas are set within the code at 1.5 times the flap chords. The camber surface designed with the WINGDES2 code for the baseline flap system is shown in figure 7. The leading- and trailing-edge design areas and the flap hinge lines are also shown on the camber-surface section drawings.

Figure 8 illustrates some quantities used in the design of cambered wings to develop the distributed thrust necessary to recover the theoretical flat-wing leading-edge thrust and, therefore, avoid undesirable leading-edge flow separation. Figure 8(a) shows a typical variation of wing-section theoretical leading-edge thrust coefficient ($c_{t,t}$) with angle of attack for a flat wing. The theoretical section thrust increases rapidly with angle of attack (as α^2) and is determined by the strength of the leading-edge singularity of the linear theory. The singularity strength

is proportional to $\Delta C_p\sqrt{x'}$, where ΔC_p is the pressure loading and x' is the distance from the leading edge. The attainable section leading-edge thrust coefficient ($c_{t,a}$) is determined by the method of reference 5. This method is based on the use of a simple sweep theory to permit a two-dimensional analysis. Then, theoretical airfoil codes are used to define thrust dependence on section geometric characteristics and limiting pressures. Finally, experimental two-dimensional airfoil data are used to define the limiting pressure dependence on local Mach number and Reynolds number. The attainable thrust coefficient equals the theoretical thrust coefficient $c_{t,t}$ up to the angle of attack $\Delta\alpha_{\text{ft}}$. The quantity $\Delta\alpha_{\text{ft}}$ is the angle-of-attack range for full leading-edge thrust. Above this angle of attack, flow separation is assumed to occur and the attainable thrust becomes a progressively smaller fraction of the full theoretical thrust. Because the induced upwash on a subsonic leading edge increases in the spanwise direction, the full thrust limit ($\Delta\alpha_{\text{ft}}$) is reached at a lower angle of attack on the more outboard wing sections. Hence, $\Delta\alpha_{\text{ft}}$ becomes progressively smaller toward the wingtip, as shown in figure 8(b).

The cambered and twisted wing thrust characteristics are similar but require the additional consideration of a quantity called the angle of zero thrust (α_{zt}). This angle can be explained with the help of figure 8(c), which shows a representative section of a cambered wing at three angles of attack. At some particular condition, shown here as $\alpha = 2°$, the tangent-on-flow condition causes both the pressure loading (ΔC_p) at the leading edge and the associated linear theory leading-edge singularity to be equal to zero. For angles on either side of this angle, linear theory predicts the occurrence of a leading-edge singularity. Thus, for the example shown here, the leading-edge thrust is zero at $\alpha = 2°$, and this is the angle of zero thrust (α_{zt}) at the span station for this section. The value of α_{zt} will generally vary across the span, and the method for calculating α_{zt} is discussed in reference 10.

For the twisted and cambered wing, the leading-edge thrust is assumed to act equally on either side of the angle of zero thrust. The variation of section thrust at a given span station would then be as shown in figure 8(d), and it is the same as that for the flat wing except that it is centered on α_{zt}. Finally, then, the angle-of-attack range for full leading-edge thrust and attached flow on a twisted and cambered wing would be between $\alpha_{\text{zt}} + \Delta\alpha_{\text{ft}}$ and $\alpha_{\text{zt}} - \Delta\alpha_{\text{ft}}$. The thrust coefficient c_t shown in figure 8(d) represents only the concentrated leading-edge thrust. The additional thrust that arises from the distribution of lifting forces over the rest of the chord is handled as part of the lifting-surface potential flow solution.

Figure 9 shows the spanwise variation of the range of full thrust for the baseline camber design of figure 7. The normal design procedure with the WINGDES2 code cambers and twists the wing so that the design angle of attack (α_{des}) equals $\alpha_{\text{zt}} + \Delta\alpha_{\text{ft}}$ across the entire span. This procedure defines the local leading-edge incidence that will develop the maximum leading-edge thrust without separation. The code also determines the shape of the optimum camber surface that will develop a distributed thrust to recover the unattained portion of the theoretical flat-wing leading-edge thrust. The wing will then have the mildest camber surface with a performance comparable to that of a flat wing with full theoretical leading-edge thrust. Figure 9 shows that, theoretically, the objective of the design process has been met with the exception of a small region near the fuselage. The computed values of $\alpha_{\text{zt}} + \Delta\alpha_{\text{ft}}$ are influenced by neighboring stations through an averaging process. Hence, the values near the wing-fuselage juncture are not entirely accurate because of the influence of the highly swept fuselage forebody. The wing-alone solution (which excludes the fuselage forebody) predicts substantially larger values of $\Delta\alpha_{\text{ft}}$ in this region of the wing. The wing-alone solution for $\alpha_{\text{zt}} + \Delta\alpha_{\text{ft}}$ essentially matches α_{des} all the way to the side of the fuselage.

The achievement of some leading-edge thrust eliminates the need for the complete alignment of the leading edge with the oncoming flow and, therefore, results in a milder camber surface and smaller flap deflections. Alternately, a design that does not account for the attainable leading-edge thrust ($t/c = 0$ in the WINGDES2 code) would have $\Delta\alpha_{\text{ft}} = 0$ and $\alpha_{\text{zt}} = \alpha_{\text{des}}$ across the span. This type of wing would have more camber or larger flap deflections and would be more conservative with regard to leading-edge separation because some margin for error would exist on each side of the design point. However, with the larger flap deflections, consideration would also have to be given to possible flow separation at the flap hinge line. (Note the load peaks at the hinge lines in fig. 1.)

Lift-drag polars and suction parameter curves for the baseline cambered wing and flat wing are shown in figure 10. The calculations were made with the WINGDES2 code and include attainable leading-edge thrust and vortex forces. The polar curves are compared with the same limits used in the definition of the suction parameter, namely, the drag of a wing with an elliptical span load distribution and the drag of a flat wing with no leading-edge thrust

or vortex forces. At the design condition, the drag of the cambered wing is close to the theoretical lower bound. The suction curves for the flat wing and cambered wing are compared with the full leading-edge thrust solution[2] (theoretical thrust) of the flat wing which has a suction parameter of 0.95. This comparison nicely illustrates the use of camber to recover the unattained part of the theoretical flat-wing leading-edge thrust with a distributed thrust.

Leading- and trailing-edge flap-deflection angles were determined from the restricted-area camber design by the method illustrated in figure 11. The original camber surface (a flat wing in the present study) is superimposed by the WINGDES2 code on the new camber surface, and the differences in leading- and trailing-edge ordinates are used to select flap-deflection angles as shown. Calculations were made to examine the effect of computational grid density on the flap deflections. The calculations were made for the various inboard leading-edge flap geometries with the 30-percent-outboard leading-edge flap. The inboard leading-edge flap deflections were found to be sensitive to grid density. The results of this study are discussed in appendix A and shown in figure A1.

Figure 12 shows the spanwise distributions of leading- and trailing-edge flap deflections calculated by the WINGDES2 code for the baseline camber design of figure 7. The increment in flow angle at the leading edge caused by the fuselage upwash was estimated from the incompressible cross-flow solution for a circular cylinder. This increment was added to the deflections computed with the WINGDES2 code. The leading-edge flap was divided into three segments. The deflection schedules for both leading- and trailing-edge flaps were selected as indicated by the solid straight lines. The inboard leading-edge flap deflection was selected to account for the large amount of upwash next to the fuselage. The oversized deflections on the other parts of that flap should not cause a problem at the leading edge because of the large range of full thrust shown in figure 9. Leading-edge flap-deflection angles much larger than the theoretical design values should, however, be moderated in consideration of possible flow separation at the flap hinge line.

The transition zone on the leading-edge flap between the inboard highly swept flap and the outboard lower swept flap may require some special attention in order to prevent flow separation. One possible method is a mechanism that would close the gap between flap segments and produce the contours shown in figure 13. Notice the break in deflection angle for the leading-edge flap located at span station B.

Although the WINGDES2 code provides a set of flap deflections that approximate the camber design, it does not make a performance analysis of the wing with deflected flaps. Performance is calculated by the design code only for the smooth camber surface. Flap-system analysis requires the use of the companion wing analysis code AERO2S. (See table V(c).) Figure 14 shows the AERO2S estimate of the range of full thrust for the chosen flap deflections of figure 12. The α_{des} from AERO2S in figure 14 is approximately 3° lower than the α_{des} from WINGDES2 in figure 9. The flat input surface for the design code was rotated $-3.24°$ in definition of an optimized surface. In an evaluation of the wing with flaps in AERO2S, no rotation was employed. (For undeflected flaps, $C_L = 0$ at $\alpha = 0°$.) Thus, the difference in α_{des} between figures 9 and 14 results from a difference in angle-of-attack reference for the two codes. Table V(c) is a sample input for the AERO2S code, and a description of the code input and output is given in reference 3.

A comparison in figure 14 of the upper range of full thrust with α_{des} provides an assessment of how well the design objectives have been met for the selected flap deflections. Here, α_{des} exceeds the upper limit of full thrust over most of the span; however, as the shaded area shows, the differences between α_{des} and the upper limit are small so that any separation and vortex development should be mild and comparable to that of a flat wing at an angle of attack of about 3°. This difference between α_{des} and the upper limit of full thrust is the result of the approximation of a smooth camber surface with deflected flaps. The low levels of separation for the uncambered deflected flaps are balanced between the leading edge and the flap hinge line. As in the case of figure 9, the wing-alone solution matches α_{des} near the fuselage.

The performance of the wing with the baseline flap deflections of figure 12 is compared in figure 15 with the performance of the whole-wing design and the restricted-area baseline camber design. At the design lift coefficient, the suction parameter of the restricted-area design is 0.92, which is only slightly lower than the theoretical ideal of 0.94 for the whole-wing design. At the same lift coefficient, the wing with deflected flaps produces a suction parameter of 0.85. A flap system that

[2]The full thrust solution was obtained from WINGDES2 by the use of a circle for the wing section ($r_{le}/c = 0.5$; $(t/c)_{max} = 1.0$) and a Reynolds number of 5×10^8. (The Reynolds number used should be as large as the computer system will permit; e.g., a Reynolds number of 10^{30} gave the same result in this case.)

more closely approximates the smooth camber shape, such as a double-hinged leading-edge flap, would perhaps develop a suction parameter closer to the cambered-wing values.

Effects of Leading-Edge Flap Planform

The flap-design procedure discussed in the preceding section was also applied to the other flap geometries shown in figure 5(b). As for the baseline case, the restricted-area designs used to define flap-deflection schedules were subject to a moment restraint from the whole-wing design ($C_{m,\text{des}} = -0.03$). The resulting spanwise deflection schedules for these flap arrangements are shown in figure 16, in which figure 16(a) shows the effect of the leading-edge flap chord at the side of the fuselage ($c_{f,\text{le,sf}}$). The outboard leading-edge flap chord ($c_{f,\text{le},o}$) is 30 percent of the wing chord. An increase in $c_{f,\text{le,sf}}$ from 0 to 16 percent chord has only a small effect on the computed deflection schedules. Figure 16(b), which shows the effect of the outboard leading-edge flap chord on the deflection schedules ($c_{f,\text{le,sf}} = 0$), shows that an increase in the outboard leading-edge flap chord results in a reduction in the required deflection angle for that flap.

The AERO2S code was used to construct performance contour plots for each of the flap systems. The results are shown in figure 17 where deflection ratios ($\delta_{\text{le},r}$ and $\delta_{\text{te},r}$) are multipliers of the selected design code deflection angles from figure 16.[3] The contour lines were drawn from solutions for various combinations of leading- and trailing-edge flap deflections. As in the case of figure 2, lines of constant pitching moment and constant angle of attack are also included. The peak value of suction parameter (without any constraint on pitching moment) is noted for each flap configuration. Notice that the peak values of suction parameter occur for larger trailing-edge deflections and smaller leading-edge deflections than those predicted by WINGDES2. (Design code values are, of course, $\delta_{\text{le},r} = \delta_{\text{te},r} = 1$.) Figure 17(a) shows that a reduction in the side of the fuselage leading-edge flap chord causes almost no loss in peak performance (maximum suction parameter). Figure 17(b) shows that maximum performance occurs for the 30-percent-chord outboard leading-edge flap. The changes in either the inboard or outboard leading-edge flap chord produce only small changes in the pitching moment and angle of attack for optimum conditions.

Comparison of Various Combinations of Baseline Flap Components

A study has been made to examine the performance of various combinations of individual flaps from the baseline flap system. Representative flap arrangements were selected to determine the relative performance of leading-edge flaps versus trailing-edge flaps and of inboard flaps versus outboard flaps. Studies of this type are useful for the identification of promising concepts for experimental study.

Results for the various combinations of flaps are shown in figures 18 to 20 and are presented in table B1 of appendix B. The AERO2S code was used to determine the optimum deflection angles and the corresponding maximum suction parameter for each flap arrangement at $C_L = 0.45$, $M = 0.20$, and the wind tunnel Reynolds number of 5.38×10^6. The performance contour plots of figure 17(a) ($c_{f,\text{le,sf}} = 0$) and figure B1 of appendix B are used to determine the flap deflections and maximum suction parameter. Bar graphs are used to compare the various configurations in figures 18 to 20. The theoretical effect on suction parameter of an increase in Reynolds number to a flight value of 200×10^6 is given both in the figures and in table B1. Note that the optimum deflection angles are for the wind tunnel Reynolds number.

Figure 18 compares results for the leading- and trailing-edge flap systems individually and together. The suction parameter and deflections were determined from figure 17(a). Results are also shown for the baseline camber design and a flat wing. The theory predicts a suction parameter of 0.31 for the flat wing at the wind tunnel Reynolds number. The trailing-edge flaps alone increase this value to 0.58, whereas leading-edge flaps alone produce a suction parameter of 0.74. Thus, for this configuration the leading-edge flaps are substantially more effective than the trailing-edge flaps.[4] The entire flap system (both leading and trailing edges) increases the suction parameter to 0.85, whereas the camber design has a value of 0.92. (These two configurations were also compared in fig. 15 for the case of design code flap deflections.) As Reynolds number increases to

[3]The optimum conditions defined by figure 17 are based on the assumption of the fixed ratio between the inboard and outboard flap deflections (for both leading and trailing edges) defined by the WINGDES2 results in figure 16. This results in a two-dimensional optimization based on $\delta_{\text{le},r}$ and $\delta_{\text{te},r}$. An optimization in which the deflections of the six flap segments were independently varied might result in a higher peak suction parameter.

[4]The supersonic cranked-wing fighter in figure 2 has the opposite result with trailing-edge flaps ($\delta_{\text{le},n} = 0$) giving higher performance than the leading-edge flaps ($\delta_{\text{te},n} = 0$).

the flight level, the suction parameter for the entire flap system increases to 0.88, which is remarkably close to the value of 0.92 for the camber design. (The Reynolds number has only a slight effect on the attached-flow camber design, as seen from table B1.) Based on the correlations between theory and experiment shown earlier in this paper and those presented in references 1 to 3 for numerous other configurations, the expectation that these performance levels can be achieved seems reasonable.

Figure 19 compares the performance of individual flap deflections. The data were obtained from figure B1 in appendix B. As illustrated by the sketches in figure 19, the two inboard trailing-edge flaps were deflected together and the two outboard leading-edge flaps were deflected together. The highest performance is produced by the leading-edge flaps and the inboard trailing-edge flaps. The outboard trailing-edge flap is the least effective and the outboard leading-edge flap is the most effective. The high-suction parameter for the leading-edge flaps is apparently due to the development of distributed thrust on the leading-edge flap. As discussed earlier in regard to sketches A and B, the increased flat-wing theoretical leading-edge thrust on the outboard parts of the wing indicates the potential for the development of more distributed thrust on the outboard portion of the leading-edge flap than on the inboard portion. The inboard trailing-edge flaps are more effective than the outboard trailing-edge flaps, perhaps because of a more favorable effect on the span load distribution.

Figure 20 compares the performance of various combinations of leading- and trailing-edge flaps. These results were obtained from both figures B1 and 17(a). The results of figure 20(a) are for the peak suction-parameter conditions and, therefore, were determined without any restraint on pitching moment. Arranged in the order of increasing suction parameter, the relative performance of these configurations reflects the same effects seen in figure 19. Configurations A and B show a higher suction parameter with the inboard trailing-edge flap than with the outboard trailing-edge flap. Configurations B and C show an increased performance with the outboard leading-edge flap relative to the inboard leading-edge flap. A comparison of configurations C, D, and E shows that the addition of the inboard leading-edge flap increases performance more than the addition of the outboard trailing-edge flap.

The aerodynamic results shown in figure 20(a) provide, of course, only a part of the information needed by the designer for the selection of the most effective flap system. A complete aircraft system study would be necessary to assess the effect of structural weight and stability and control on the takeoff and landing performance and engine noise levels. These types of studies could, for example, examine the effectiveness of the inboard leading-edge flap by comparing the benefits of the increased aerodynamic performance of configuration F with the reduced structural weight and complexity of configuration D.

Note that the majority of the correlations between the AERO2S theory and experimental results have been made for essentially full-span flaps (refs. 1 to 3). Therefore, some additional experimental verification of the theory should be made for cases that involve individual flap deflections, such as those shown in figures 19 and 20(a).

Optimum flap deflections for the configurations of figure 20(a) were also determined with a pitching-moment constraint of $C_m = 0$. The results are shown in figure 20(b) in which the configurations are arranged in the same order as in figure 20(a). These results correspond to the highest suction parameter along the $C_m = 0$ line in figures B1 and 17(a). The pitching-moment constraint has decreased the performance of every configuration.

A curious situation is noted for configurations E and F. Presumably, the performance of an optimized four-flap system would, under no circumstance, be poorer than that of an optimized three-flap system. However, this has occurred in the present case because of the previously mentioned assumption that fixes the ratio between the inboard and outboard flap deflections at the value established by the design code. A truly optimized solution with moment restraint could easily call for a negative outboard flap deflection. A more accurate version of figure 20(b) could have been made by starting with the design code WINGDES2 with the moment restraint applied and with NTES = 4 so as to allow a greater spanwise variation of the trailing-edge deflection. For the purposes of this paper, however, this is not necessary. The present example serves to illustrate how aircraft trim considerations may change the relative merits of the various candidate flap systems, and how the code can be used to provide trade-off data for design studies that take trim considerations into account.

Conclusions

A study of subsonic flap systems for supersonic cruise commercial aircraft has been conducted by the use of linear attached-flow theory modified to account

for the effects of attainable leading-edge thrust and vortex forces that arise because of leading-edge flow separation. This approach is based on the concept that a high level of aerodynamic efficiency requires a flow that is as nearly attached as possible. The design conditions were a Mach number of 0.20 and a lift coefficient of 0.45.

The conclusions of this study are as follows:

1. The modified linear theory methods provide a useful preliminary design tool for subsonic flap systems. Computer programs based on modified linear theory methods require little effort in preparation of input data and have short execution times.
2. Correlations of theory and experiment show that the theory provides a good estimate of the required leading- and trailing-edge flap deflections for optimum performance and gives a conservative estimate of the level of performance.
3. Theoretical performance levels of 85 percent of full suction or greater should be achievable with simple hinged or plain flaps. The required flap geometry can be defined from optimized smooth camber surfaces designed for restricted areas of the wing at the leading and trailing edges.
4. Flap deflections for optimum performance from the wing design code require the use of a constraint on pitching moment obtained from a whole-wing solution.
5. A substantial reduction in flap chord at the side of the fuselage on the inboard leading-edge flap was found to have a minor effect on the optimum leading- and trailing-edge flap deflections and on the maximum performance.
6. Variation of the outboard leading-edge flap chord showed that maximum performance was achieved when this flap chord was approximately 30 percent of the wing chord.
7. The modified linear theory can be used to compare the aerodynamic performance of various flap systems that have optimized flap-deflection angles; however, the selection of the flap system that provides the best takeoff and landing characteristics would have to be made on the basis of a study of the complete aircraft system.

NASA Langley Research Center
Hampton, VA 23681-0001
June 21, 1994

Appendix A

Design Solution Convergence

The density of the grid used for the numerical solution in the WINGDES2 and AERO2S codes is determined by the parameters JBYMAX (the number of spanwise elements) and ELAR (the element aspect ratio). Figure A1 shows the effect of these parameters on the spanwise distribution of baseline leading-edge flap deflection from WINGDES2. These calculations were made for the design conditions of this study with a slight adjustment to the design pitching-moment coefficient ($C_{m,\text{des}}$). The value of $C_{m,\text{des}}$ varied somewhat with grid density, and a value of $C_{m,\text{des}} = -0.04$ was used for this convergence study. The spanwise distribution of the number of elements on the leading-edge flap is also shown. Guidelines given in references 2 and 3 suggest at least two elements on the leading- and trailing-edge flaps. Maintaining two elements at every span station of the baseline leading-edge flap is not possible because the flap chord goes to zero at the side of the fuselage. However, the results of figure A1 indicate that the distribution of flap deflection is essentially converged for JBYMAX = 18 and ELAR = 2. These values were used for the majority of the calculations in both the WINGDES2 and the AERO2S codes. In the case of the 20-percent-chord outboard leading-edge flap, the value of ELAR was increased to 3.

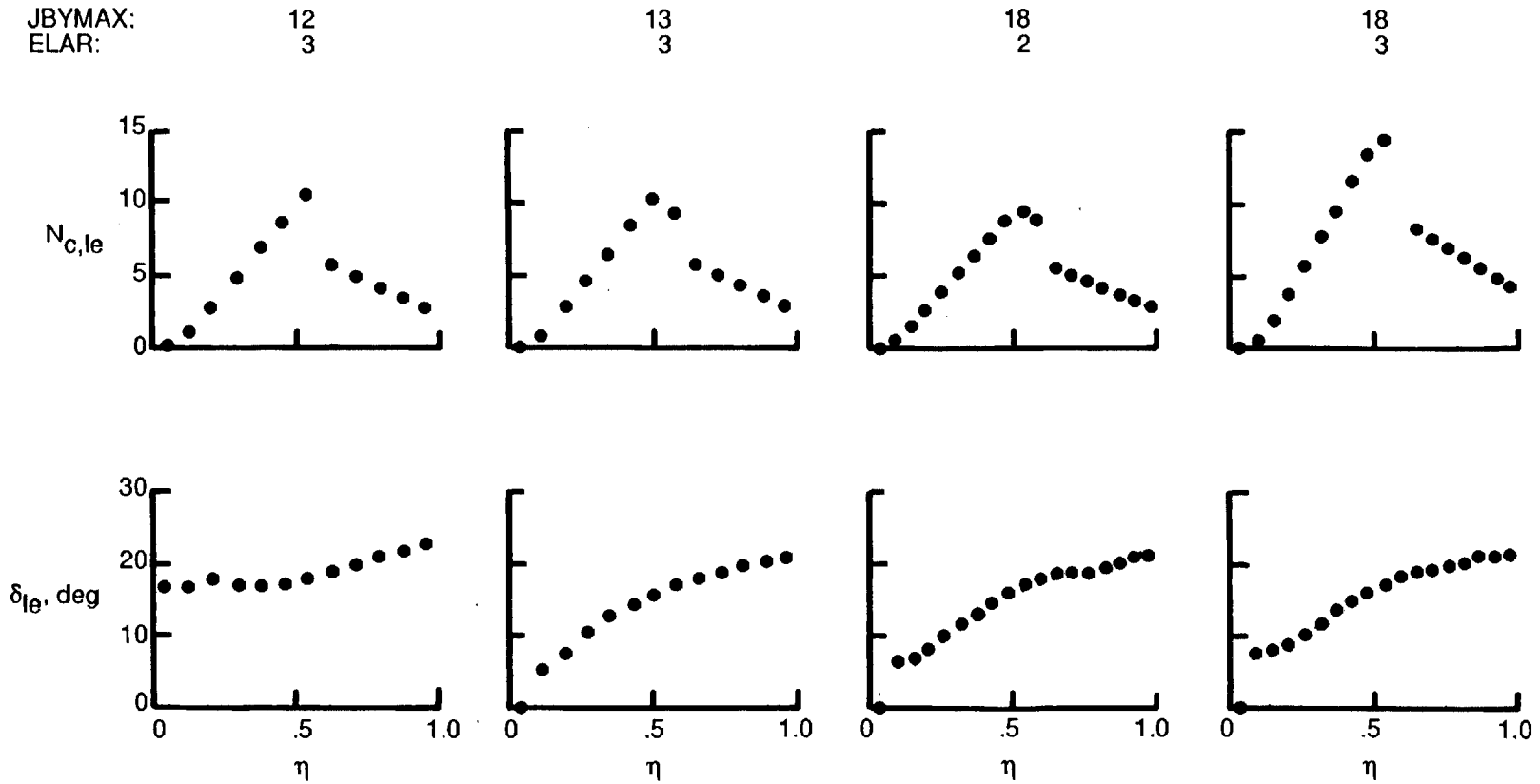

Figure A1. Sample of data used in study of design solution convergence. Baseline flaps: $c_{f,\mathrm{le},o} = 0.30c$, $c_{f,\mathrm{le,sf}} = 0$. $M = 0.20$; $C_{L,\mathrm{des}} = 0.45$; $C_{m,\mathrm{des}} = -0.04$.

Appendix B

Performance of Various Combinations of Baseline Flap Components

Performance contour plots are shown in figure B1 for various combinations of flaps from the baseline flap system. The conditions are $C_L = 0.45$, $M = 0.20$, and $R = 5.38 \times 10^6$. The nominal deflection schedules ($\delta_{\mathrm{le},r} = \delta_{\mathrm{te},r} = 1$) were obtained from restricted-area wing designs with a whole-wing design C_m of -0.03. Because this is not necessarily an appropriate procedure when large areas of the leading and/or trailing edge are left out of the design, optimum deflections may differ significantly from the nominal values. A fixed ratio between the inboard and outboard flap deflections from the design code was assumed, as in the case of figure 17 of the main text. Optimum deflection angles and the corresponding maximum suction parameter for each flap arrangement were determined from figure B1 and from the baseline performance contour plot in figure 17(a). The results are presented in table B1 and are plotted in figures 18 to 20 of the main text. The change in maximum suction parameter as Reynolds number increased to 200×10^6 was calculated for each case, and the results are included in table B1 and in figures 18 to 20. Note that the optimum deflection angles are for the wind tunnel Reynolds number of 5.38×10^6.

Table B1. Optimum Deflection Schedules for Various Combinations of Baseline Flap Components at a Lift Coefficient of 0.45 and a Mach Number of 0.20

[Results are given in order of magnitude of suction parameter for $R = 5.38 \times 10^6$]

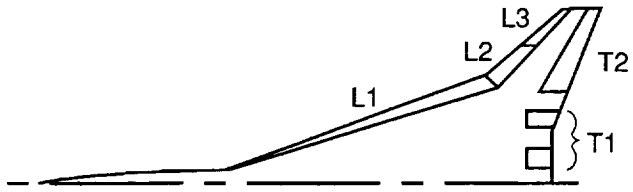

(a) Both leading- and trailing-edge deflections with no pitching-moment constraint

Deflections, deg, for flaps—					Suction parameters, S_s, for—	
L1	L2	L3	T1	T2	$R = 5.38 \times 10^6$	$R = 200 \times 10^6$
18	21	23	12	10	0.85	0.88
18	23	23	16	0	.81	.84
17	23	26	0	10	.77	.83
0	19	22	17	14	.74	.80
0	19	22	21	0	.66	.72
16	0	0	16	14	.65	.69
0	22	24	0	13	.61	.69
19	0	0	20	0	.61	.69
19	0	0	0	10	.53	.58

(b) Both leading- and trailing-edge deflections when trimmed to $C_m = 0$

Deflections, deg, for flaps—					Suction parameters, S_s, for—	
L1	L2	L3	T1	T2	$R = 5.38 \times 10^6$	$R = 200 \times 10^6$
19	25	25	10	0	0.80	0.83
20	24	26	4	3	.79	.82
17	23	26	0	6	.76	.83
0	22	24	5	4	.63	.70
0	22	25	14	0	.63	.70
0	22	24	0	8	.59	.67
19	0	0	5	0	.53	.60
19	0	0	2	2	.52	.58
19	0	0	0	3	.50	.56

(c) Smooth cambered flaps compared with leading-edge, trailing-edge, and individual deflections, and with flat (uncambered) wing

Deflections, deg, for flaps—					Suction parameters, S_s, for—	
L1	L2	L3	T1	T2	$R = 5.38 \times 10^6$	$R = 200 \times 10^6$
Smooth cambered flaps					0.920	0.926
22	24	27	0	0	0.74	0.81
0	0	0	18	15	.58	.65
0	22	24	0	0	.52	.60
0	0	0	23	0	.50	.58
20	0	0	0	0	.49	.55
0	0	0	0	13	.40	.48
Flat (uncambered) wing					0.313	0.410

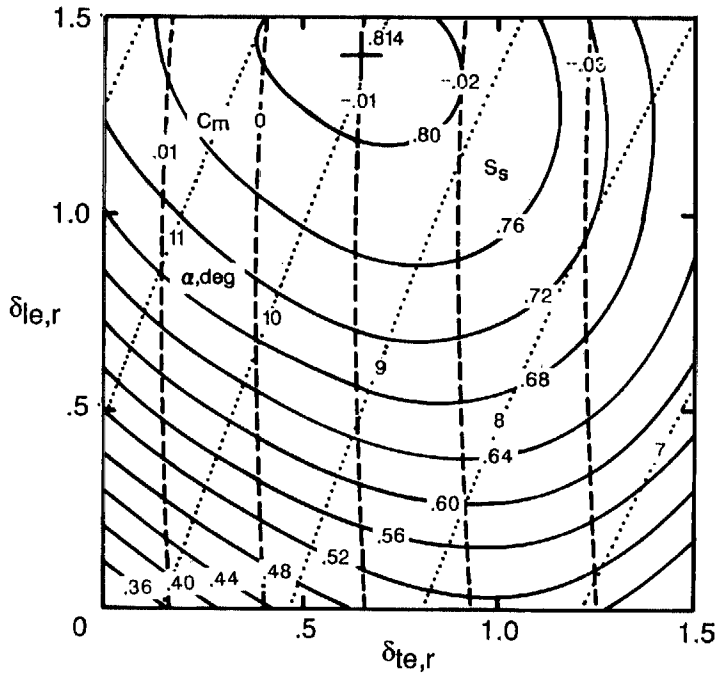

(a) All leading edge and inboard trailing-edge flaps. $\delta_{le,r} = 1$ is for $\delta_{le} = 13°$, 17°, and 17° for L1, L2, and L3, respectively. $\delta_{te,r} = 1$ is for $\delta_{te} = 24°$ and 0° for T1 and T2, respectively.

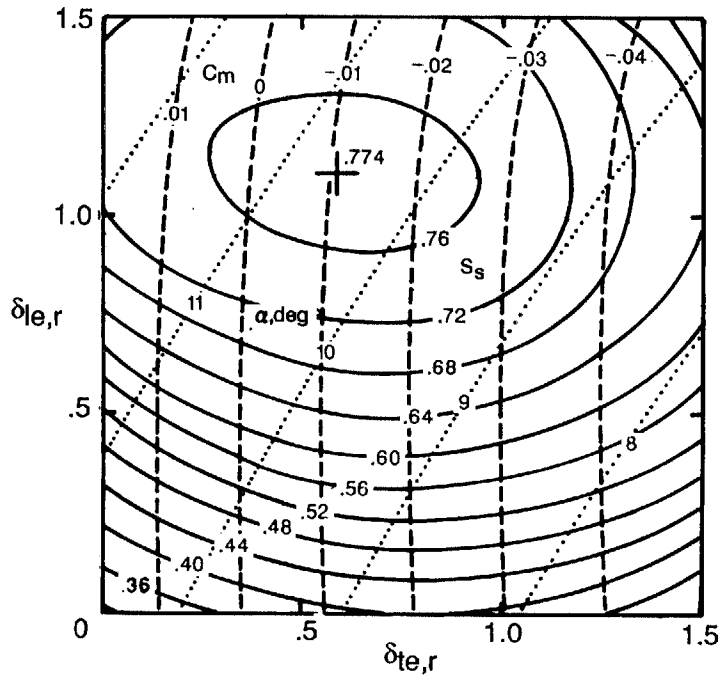

(b) All leading edge and outboard trailing-edge flaps. $\delta_{le,r} = 1$ is for $\delta_{le} = 15°$, 21°, and 24° for L1, L2, and L3, respectively. $\delta_{te,r} = 1$ is for $\delta_{te} = 0°$ and 16° for T1 and T2, respectively.

Figure B1. Performance contour maps for various combinations of leading- and trailing-edge flaps for baseline flap geometry. $M = 0.20$; $C_L = 0.45$; $R = 5.38 \times 10^6$.

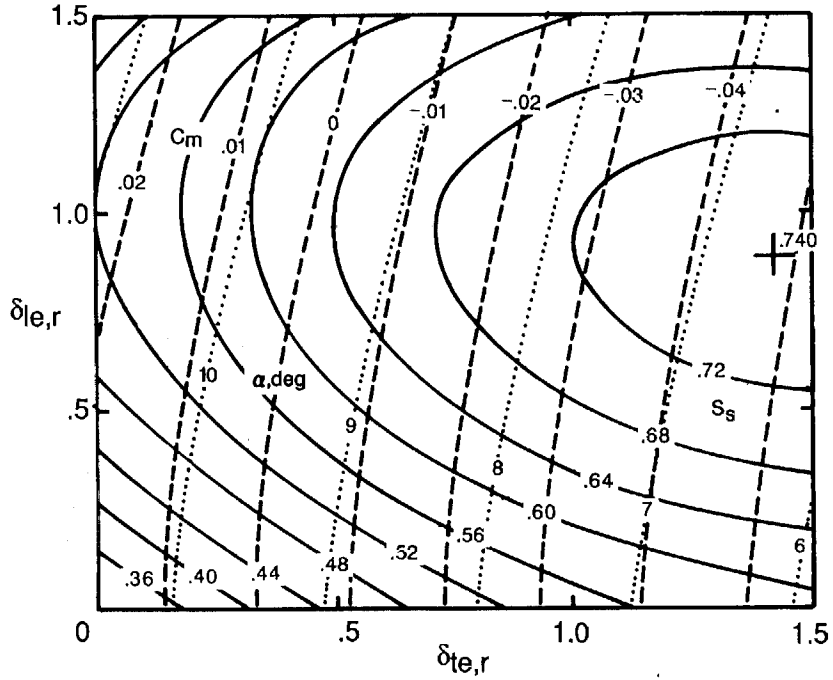

(c) Outboard leading-edge and all trailing-edge flaps. $\delta_{le,r} = 1$ is for $\delta_{le} = 0°$, 22°, and 24° for L1, L2, and L3, respectively. $\delta_{te,r} = 1$ is for $\delta_{te} = 12°$ and 10° for T1 and T2, respectively.

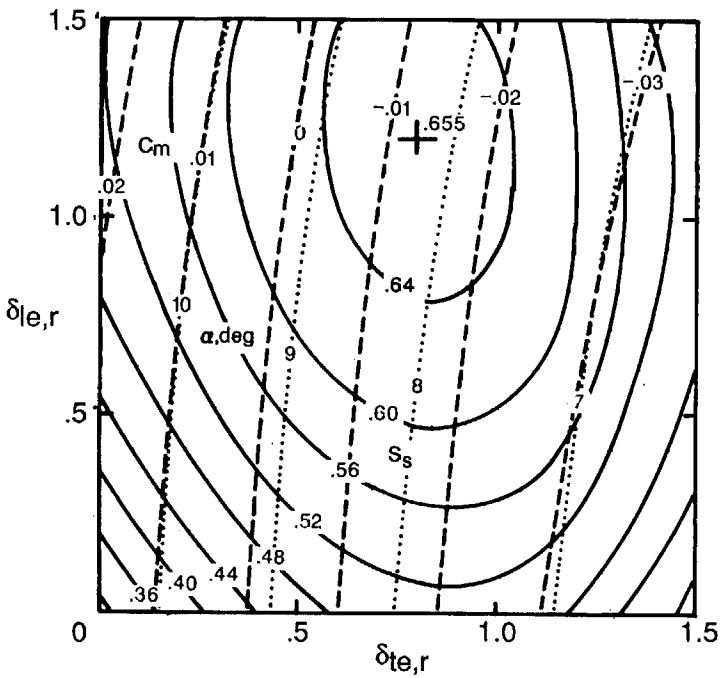

(d) Outboard leading-edge and inboard trailing-edge flaps. $\delta_{le,r} = 1$ is for $\delta_{le} = 0°$, 16°, and 18° for L1, L2, and L3, respectively. $\delta_{te,r} = 1$ is for $\delta_{te} = 26°$ and 0° for T1 and T2, respectively.

Figure B1. Continued.

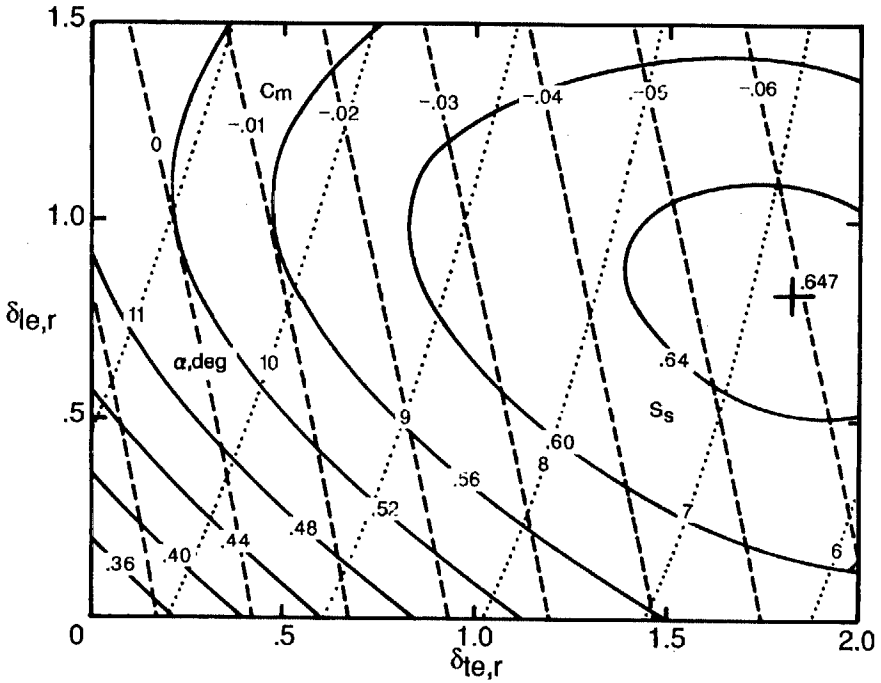

(e) Inboard leading-edge and all trailing-edge flaps. $\delta_{le,r} = 1$ is for $\delta_{le} = 19°$, 0°, and 0° for L1, L2, and L3, respectively. $\delta_{te,r} = 1$ is for $\delta_{te} = 9°$ and 8° for T1 and T2, respectively.

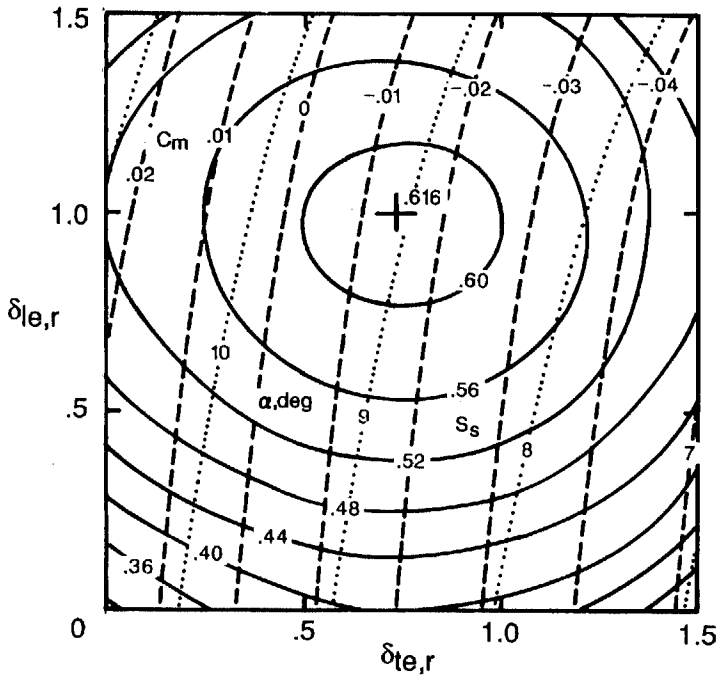

(f) Outboard leading-edge and trailing-edge flaps. $\delta_{le,r} = 1$ is for $\delta_{le} = 0°$, 22°, and 24° for L1, L2, and L3, respectively. $\delta_{te,r} = 1$ is for $\delta_{te} = 0°$ and 17° for T1 and T2, respectively.

Figure B1. Continued.

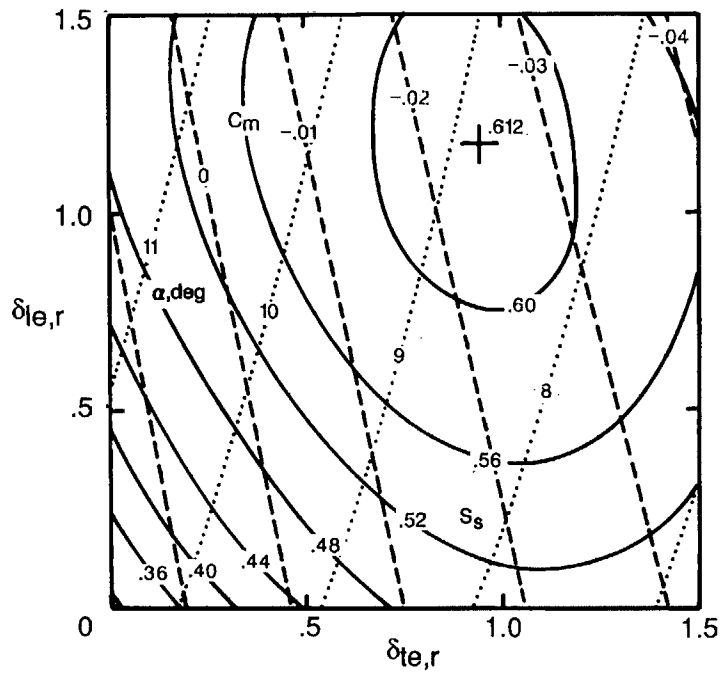

(g) Inboard leading-edge and trailing-edge flaps. $\delta_{le,r} = 1$ is for $\delta_{le} = 16°$, 0°, and 0° for L1, L2, and L3, respectively. $\delta_{te,r} = 1$ is for $\delta_{te} = 21°$ and 0° for T1 and T2, respectively.

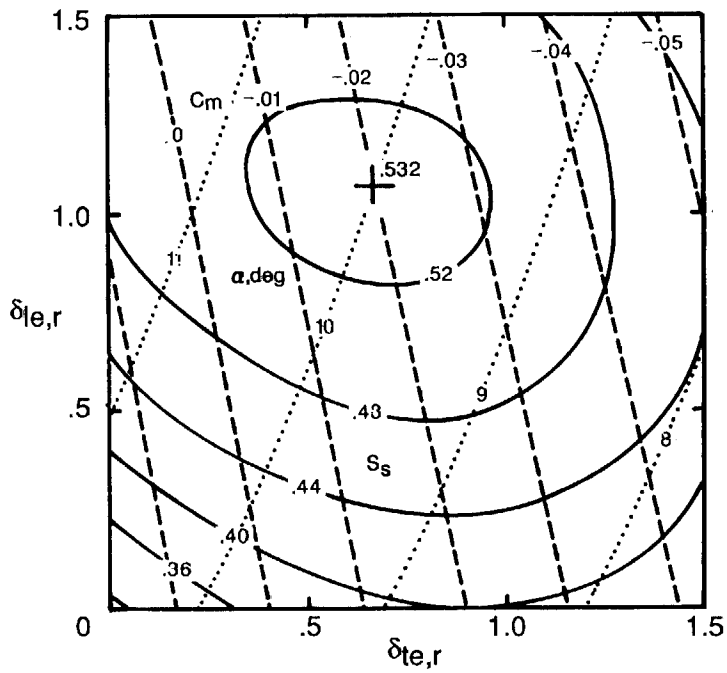

(h) Inboard leading-edge and outboard trailing-edge flaps. $\delta_{le,r} = 1$ is for $\delta_{le} = 18°$, 0°, and 0° for L1, L2, and L3, respectively. $\delta_{te,r} = 1$ is for $\delta_{te} = 0°$ and 14° for T1 and T2, respectively.

Figure B1. Concluded.

References

1. Carlson, Harry W.; and Darden, Christine M.: *Applicability of Linearized-Theory Attached-Flow Methods to Design and Analysis of Flap Systems at Low Speeds for Thin Swept Wings With Sharp Leading Edges.* NASA TP-2653, 1987.

2. Carlson, Harry W.; and Darden, Christine M.: *Validation of a Pair of Computer Codes for Estimation and Optimization of Subsonic Aerodynamic Performance of Simple Hinged-Flap Systems for Thin Swept Wings.* NASA TP-2828, 1988.

3. Carlson, Harry W.; Darden, Christine M.; and Mann, Michael J.: *Validation of a Computer Code for Analysis of Subsonic Aerodynamic Performance of Wings With Flaps in Combination With a Canard or Horizontal Tail and an Application to Optimization.* NASA TP-2961, 1990.

4. Polhamus, Edward C.: Predictions of Vortex-Lift Characteristics by a Leading-Edge Suction Analogy. *J. Aircr.*, vol. 8, no. 4, Apr. 1971, pp. 193–199.

5. Carlson, Harry W.; Mack, Robert J.; and Barger, Raymond L.: *Estimation of Attainable Leading-Edge Thrust for Wings at Subsonic and Supersonic Speeds.* NASA TP-1500, 1979.

6. Carlson, Harry W.; and Walkley, Kenneth B.: *Numerical Methods and a Computer Program for Subsonic and Supersonic Aerodynamic Design and Analysis of Wings With Attainable Thrust Considerations.* NASA CR-3808, 1984.

7. Campbell, Bryan A.; Hom, Kam W.; and Huffman, Jarrett K.: *Investigation of Subsonic Maneuver Performance of a Supersonic Fighter Cranked Wing.* NASA TP-2687, 1987.

8. Scott, Samuel J.; Nicks, Oran W.; and Imbrie, P. K.: *Effects of Leading-Edge Devices on the Low-Speed Aerodynamic Characteristics of a Highly-Swept Arrow-Wing.* NASA CR-172531, 1985.

9. Patterson, Elizabeth W.; and Braslow, Albert L.: *Ordinates and Theoretical Pressure-Distribution Data for NACA 6- and 6A-Series Airfoil Sections With Thicknesses From 2 to 21 and From 2 to 15 Percent Chord, Respectively.* NASA TR R-84, 1961. (Supersedes NACA TN 4322.)

10. Carlson, Harry W.; and Mann, Michael J.: *Survey and Analysis of Research on Supersonic Drag-Due-to-Lift Minimization With Recommendations for Wing Design.* NASA TP-3202, 1992.

Table I. Geometric Characteristics of Wing Planform Extended to Configuration Centerline

Area, in^2	1584.72
Aspect ratio	2.05
Taper ratio	0.10
Leading-edge sweep, inboard, deg	71
Leading-edge sweep, outboard, deg	50
Span, in.	57.0
Root chord, in.	63.46
Tip chord, in.	6.35
Mean aerodynamic chord, in.	38.86
Length, in.	71.14

Table II. Properties of Wing Sections

y, in.	$(t/c)_{max}$	x'/c for $(t/c)_{max}$	r_{le}/c
0	0.026	0.50	0.00048
1.24	.025	.50	.00045
2.48	.031	.50	.00066
4.96	.028	.475	.00055
9.92	.023	.53	.00038
13.61	.022	.45	.00035
18.0	.027	.45	.00051
21.0	.026	.50	.00048
24.0	.026	.50	.00048
28.5	.030	.50	.00062

Table III. Coordinates of Configuration Planform

(a) Leading edge

y, in.	x_{le}, in.
0	0
1.31	11.733
2.30	29.994
18.00	75.590
28.50	88.103

(b) Trailing edge

y, in.	x_{te}, in.
0	86.766
8.28	86.594
13.608	88.051
28.50	94.453

Table IV. Definition of Flap Planforms

(a) Leading-edge flap systems

$c_{f,\mathrm{le,sf}}$, percent c	$c_{f,\mathrm{le},o}$, percent c	y, in.	$c_{f,\mathrm{le}}$, in.
0	20	2.3	0
		15.02	8.66
		18.0	2.92
		28.5	1.27
0	30	2.3	0
		15.9	8.50
		18.0	4.30
		28.5	1.91
0	40	2.3	0
		16.7	8.50
		18.0	5.80
		28.5	2.54
8	30	2.3	4.6
		15.9	8.50
		18.0	4.30
		28.5	1.91
16	30	2.3	9.2
		15.9	8.50
		18.0	4.30
		28.5	1.91

(b) Trailing-edge flap system

y, in.	$c_{f,\mathrm{te}}$, in.
2.40	4.46
6.23	4.50
9.48	4.80
12.00	5.40
15.01	4.50
28.50	1.95

Table V. Sample of Computer Code Input Data

[Refs. 3 and 10 give a more complete description of code input and output data]

(a) WINGDES2 code for whole-wing design

```
HIGH SPEED CIVIL TRANSPORT - HSCT-71-50 - SUBSONIC WHOLE WING DESIGN
$INPT1
NLEY=5,TBLEY=0.000,1.3100,2.3000,18.000,28.500,
       TBLEX=0.000,11.733,29.994,75.590,88.103,
NTEY=4,TBTEY=0.0000,8.2800,13.608,28.500,
       TBTEX=86.766,86.594,88.051,94.453,
XMAX=94.453,
SREF=1584.72,
CBAR=38.8633,
XMC=69.120,
ELAR=2.0,
JBYMAX=18,
NYR=10,TBYR=0.00000,1.24000,2.48000,4.96000,9.92000,13.6100,18.0000,
            21.0000,24.0000,28.5000,
      TBTOC=0.02600,0.02500,0.03100,0.02800,0.02300,0.02200,0.02700,
            0.02600,0.02600,0.03000,
      TBETA=0.50000,0.50000,0.50000,0.47500,0.53000,0.45000,0.45000,
            0.50000,0.50000,0.50000,
      TBROC=0.00048,0.00045,0.00066,0.00055,0.00038,0.00035,0.00051,
            0.00048,0.00048,0.00062,
IVOROP=1, IPRSLD=0,
XM=0.2, RN=5.38,
NALPHA=12, TALPHA=-2.0,0.0,2.0,4.0,6.0,8.0,10.0,12.0,14.0,16.0,
                  18.0,20.0,
CLDES=0.45,
NLEC=4, TBLECY=0.000,2.30,18.00,28.50,
        TBLEC=86.77,56.7,14.30,6.350,
IAFIX=1,
TAFIX=11.69,14.06,12.90,13.66,16.23,19.14,22.08,25.26,28.80,
     32.05,34.04,34.11,33.34,32.90,32.86,32.99,32.96,32.99,
$
```

Table V. Continued

(b) WINGDES2 code for restricted-area design for leading- and trailing-edge flaps; leading-edge flap of 0.30c on outboard panel and tapers to zero chord at side of fuselage

```
HSCT-71-50 - RESTRIC DES - LE flap 30% c outbd, taper to 0 at root
$INPT1
NLEY=5,TBLEY=0.000,1.3100,2.3000,18.000,28.500,
       TBLEX=0.000,11.733,29.994,75.590,88.103,
NTEY=4,TBTEY=0.0000,8.2800,13.608,28.500,
       TBTEX=86.766,86.594,88.051,94.453,
XMAX=94.453,
SREF=1584.72,
CBAR=38.8633,
XMC=69.120,
ELAR=2.0,
JBYMAX=18,
NYR=10,TBYR=0.00000,1.24000,2.48000,4.96000,9.92000,13.6100,18.0000,
            21.0000,24.0000,28.5000,
      TBTOC=0.02600,0.02500,0.03100,0.02800,0.02300,0.02200,0.02700,
            0.02600,0.02600,0.03000,
      TBETA=0.50000,0.50000,0.50000,0.47500,0.53000,0.45000,0.45000,
            0.50000,0.50000,0.50000,
      TBROC=0.00048,0.00045,0.00066,0.00055,0.00038,0.00035,0.00051,
            0.00048,0.00048,0.00062,
IVOROP=1, IPRSLD=0,
XM=0.2, RN=5.38,
NALPHA=12, TALPHA=-2.0,0.0,2.0,4.0,6.0,8.0,10.0,12.0,14.0,16.0,
                  18.0,20.0,
CLDES=0.45, CMDES=-0.03,
IFLPDES=1,
NGCS=0,
NLEC=6, TBLECY=0.0,2.29,2.300,15.9,18.0,28.5,
        TBLEC=0.0,0.00,0.001,8.50,4.30,1.91,
NTES=2,
NTEC=12,TBTECY=0.000,2.390,2.400,6.230,6.240,9.470,9.480,12.00,
               12.01,15.00,15.01,28.50,
        TBTEC=0.000,0.000,4.460,4.500,0.000,0.000,4.800,5.400,
               0.000,0.000,4.500,1.950,
IAFIX=1,
TAFIX=0.000,17.06,20.13,22.80,27.13,30.92,33.82,36.47,39.23,
      41.72,43.91,44.79,45.07,45.93,47.44,49.11,50.57,52.10,
$
```

Table V. Concluded

(c) AERO2S analysis code; leading-edge flap of 0.30c on outboard panel and tapers to zero chord at side of fuselage

```
HSCT-71-50 LE&TE FLAP ANAL -AERO2S-LE 30% OUTBD, TAPER TO 0.0 AT ROOT
$INPT1
NLEY=5,TBLEY=0.000,1.3100,2.3000,18.000,28.500,
       TBLEX=0.000,11.733,29.994,75.590,88.103,
NTEY=4,TBTEY=0.0000,8.2800,13.608,28.500,
       TBTEX=86.766,86.594,88.051,94.453,
XMAX=94.453,
SREF=1584.72,
CBAR=38.8633,
XMC=69.120,
ELAR=2.0,
JBYMAX=18,
NYC=2,TBYC=0.,28.5,NPCTC=2,TBPCTC=0.,100.,TZORDC=52*0.0,
NYR=10,TBYR=0.00000,1.24000,2.48000,4.96000,9.92000,13.6100,18.0000,
            21.0000,24.0000,28.5000,
      TBTOC=0.02600,0.02500,0.03100,0.02800,0.02300,0.02200,0.02700,
            0.02600,0.02600,0.03000,
      TBETA=0.50000,0.50000,0.50000,0.47500,0.53000,0.45000,0.45000,
            0.50000,0.50000,0.50000,
      TBROC=0.00048,0.00045,0.00066,0.00055,0.00038,0.00035,0.00051,
            0.00048,0.00048,0.00062,
IVOROP=1, IPRSLDA=1,
XM=0.2, RN=5.38,
NALPHA=12, TALPHA=-2.0,0.0,2.0,4.0,6.0,8.0,10.0,12.0,14.0,16.0,
                  18.0,20.0,
NLEFY=12,TBLEFY=0.000,2.300,2.310,8.500,8.510,15.90,15.91,18.00,
                18.01,23.00,23.01,28.50,
         TBLEFC=0.000,0.000,0.001,3.950,3.950,8.500,8.500,4.300,
                4.300,3.140,3.140,1.910,
         TBLEFD=0.000,0.000,19.00,19.00,19.00,19.00,19.00,22.00,
                22.00,22.00,24.00,24.00,
NTEFY=12,TBTEFY=0.000,2.400,2.410,6.230,6.240,9.470,9.480,12.00,
                12.01,15.00,15.01,28.50,
         TBTEFC=0.000,0.000,4.460,4.500,0.000,0.000,4.800,5.400,
                0.000,0.000,4.500,1.910,
         TBTEFD=0.000,0.000,11.00,11.00,0.000,0.000,11.00,11.00,
                0.000,0.000,9.000,9.000,
         NADLEFD=1,TXMLEFD=0.0,
         NADTEFD=1,TXMTEFD=0.0,
CLDES=0.45,
$
```

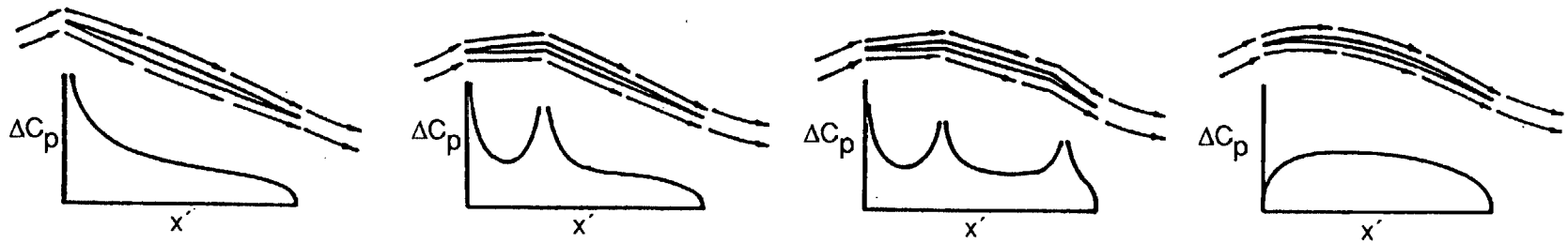

(a) Theoretical attached flow.

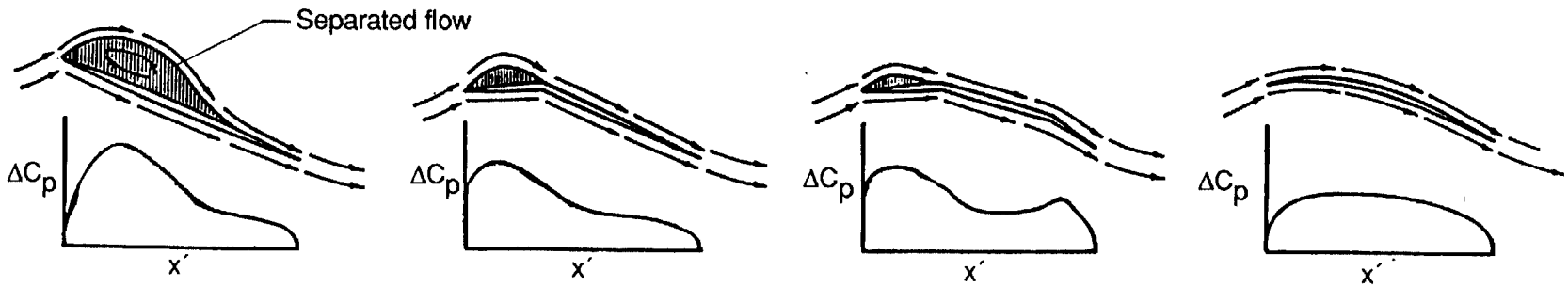

(b) Real flow with separation.

Figure 1. Comparison of theoretical attached-flow solution with actual or real separated flow for several wing profiles.

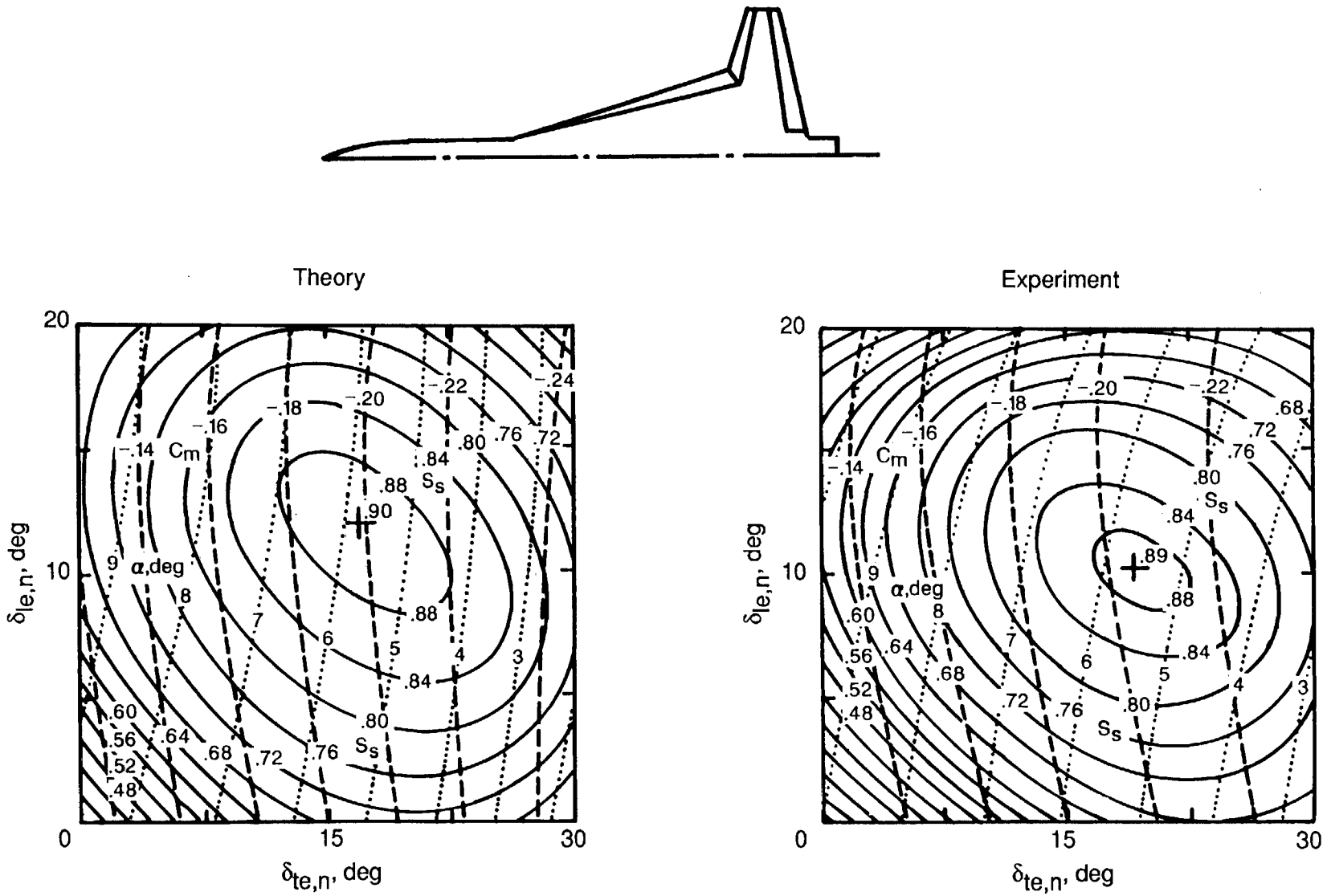

Figure 2. Predicted and measured performance map for flap system of supersonic cranked-wing fighter. $C_L = 0.45$; $M = 0.50$; $R = 2.9 \times 10^6$.

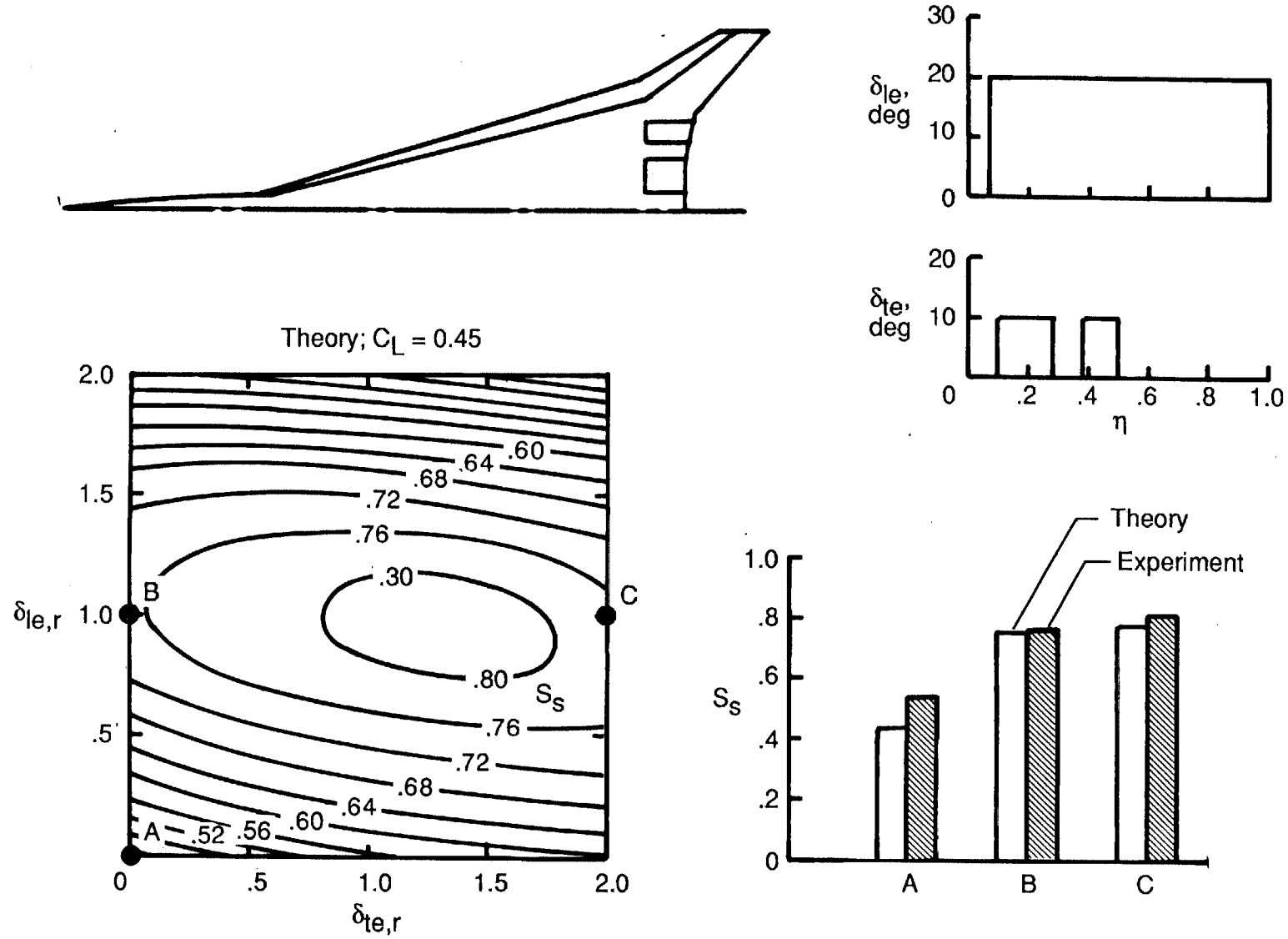

(a) Inboard leading-edge flap with small chord.

Figure 3. Predicted and measured performance for flap systems on arrow-wing supersonic transport. $C_L = 0.45$; $M = 0.21$; $R = 4.1 \times 10^6$.

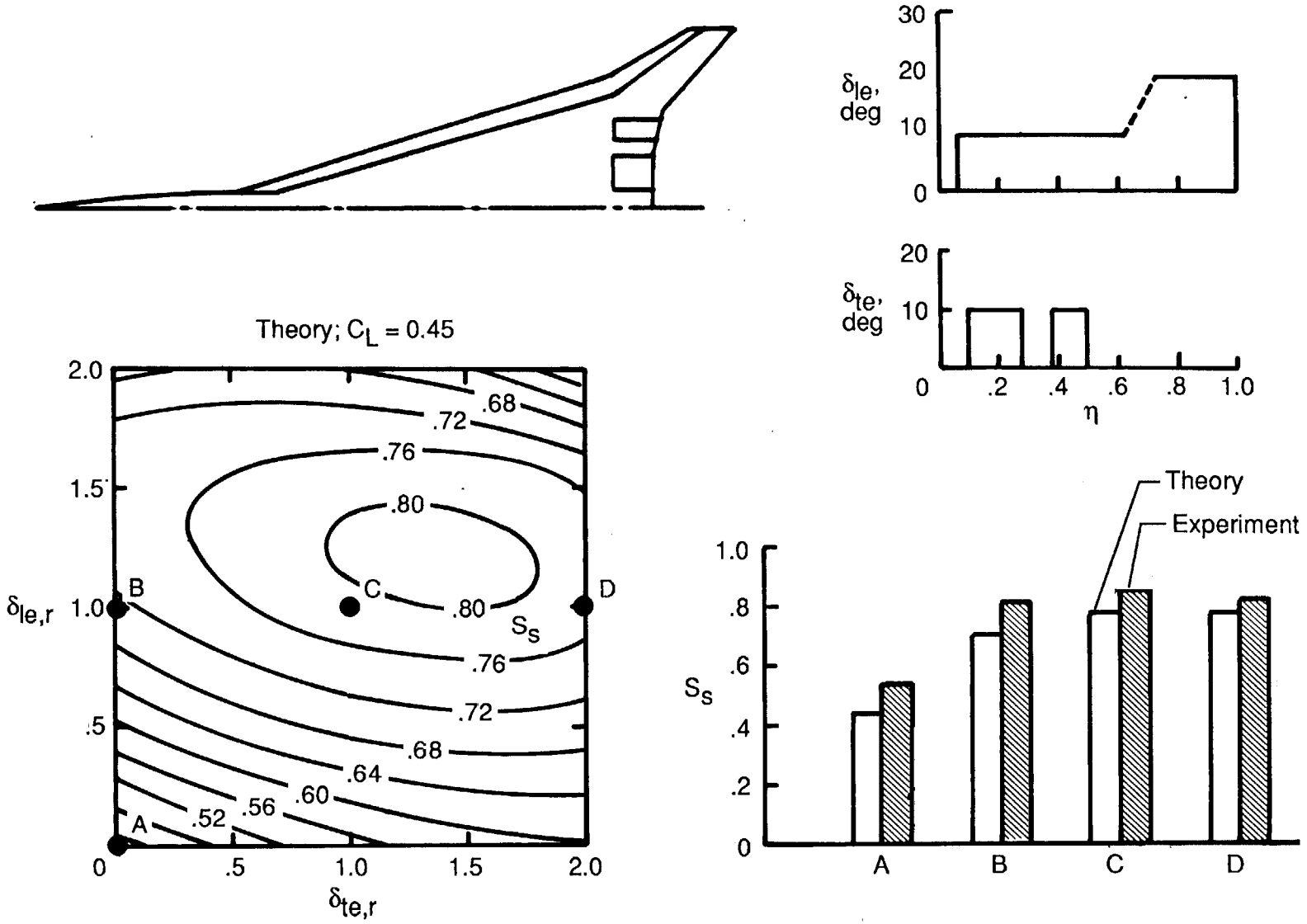

(b) Inboard leading-edge flap with moderate chord.

Figure 3. Concluded.

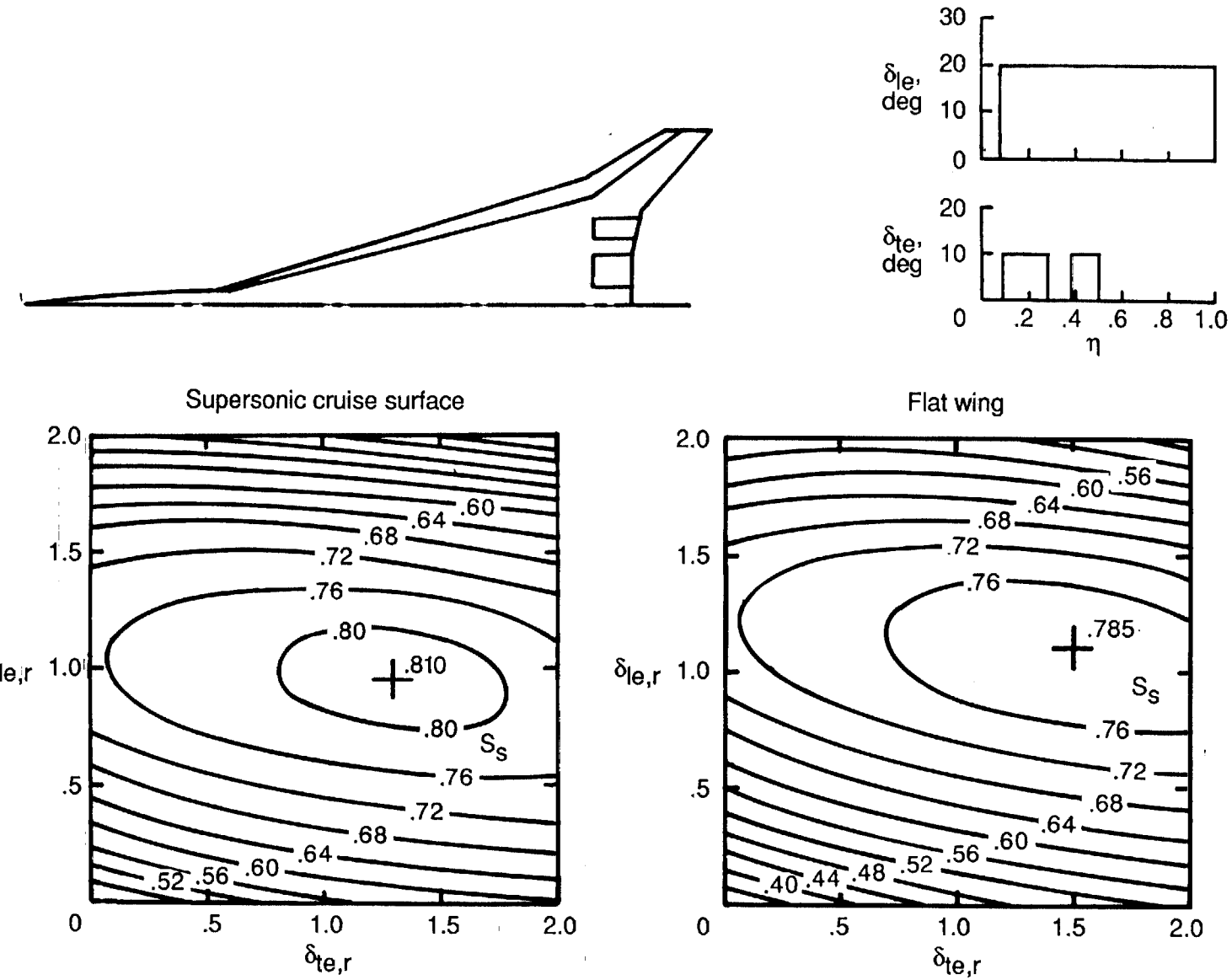

Figure 4. Comparison of theoretical performance of flap systems for flat-wing surface and supersonic cruise surface of arrow-wing supersonic transport of figure 3(a). $C_L = 0.45$; $M = 0.21$.

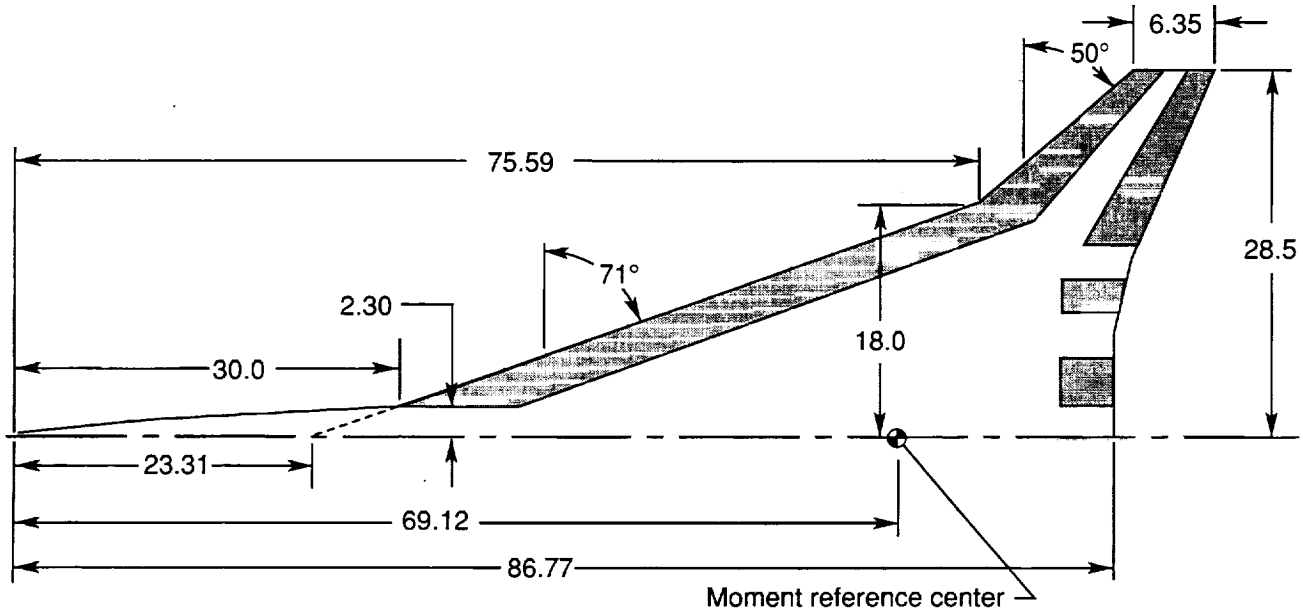

(a) General arrangement of configurations.

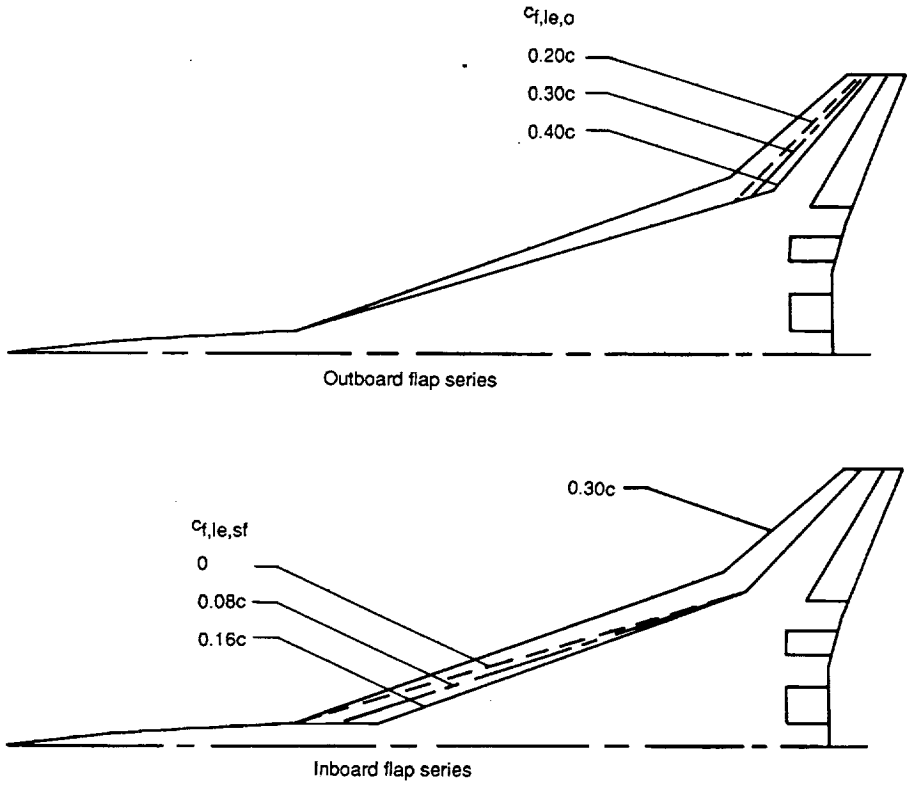

(b) Leading-edge flap planforms showing flap hinge lines.

Figure 5. Geometric characteristics of present configuration. Shaded areas show regions of wing available for installation of flaps. Linear dimensions are given in inches.

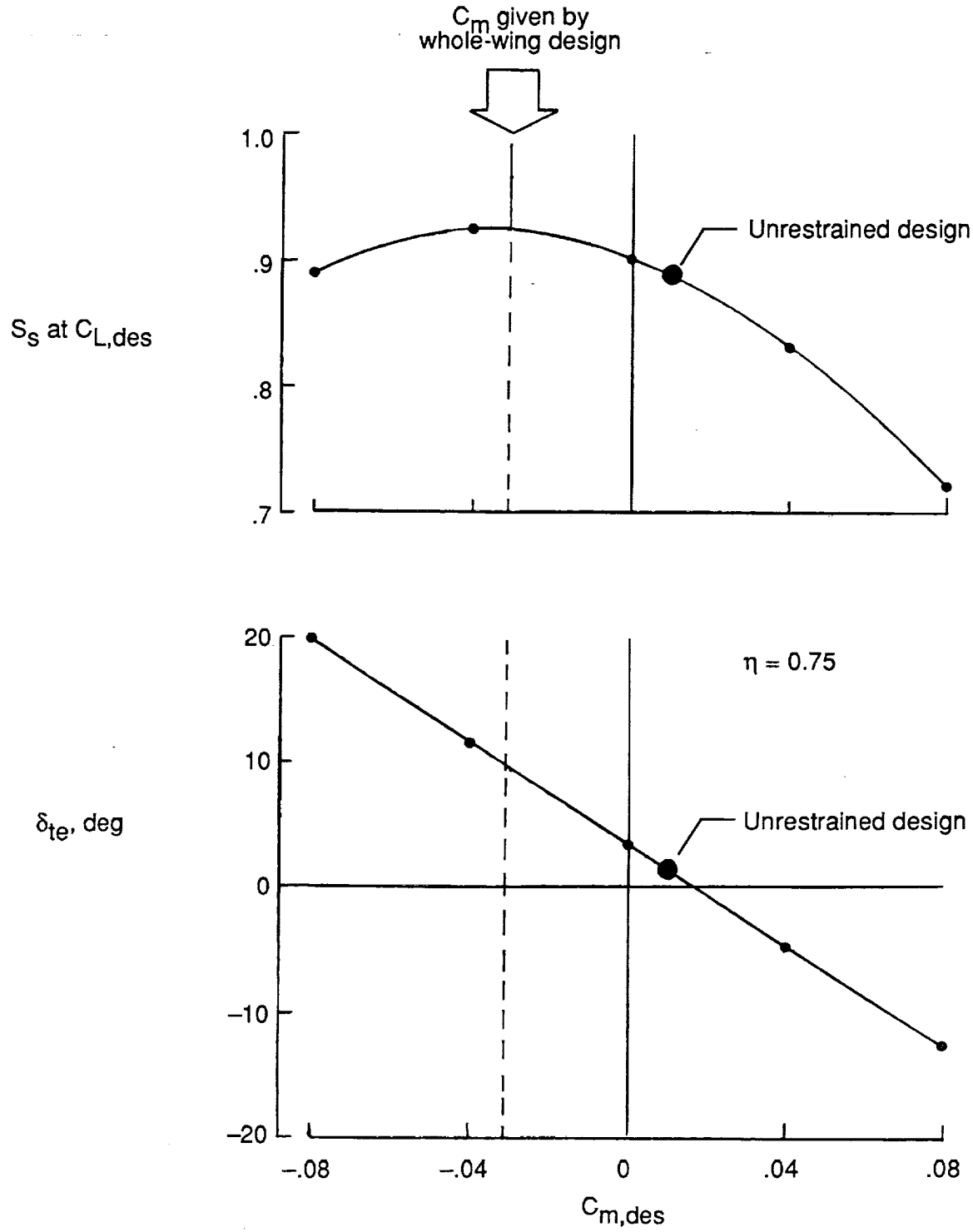

Figure 6. Effect of pitching-moment constraint on restricted-area wing design for baseline case. $c_{f,\mathrm{le},o} = 0.30c$; $c_{f,\mathrm{le,sf}} = 0$; $M = 0.20$; $C_{L,\mathrm{des}} = 0.45$.

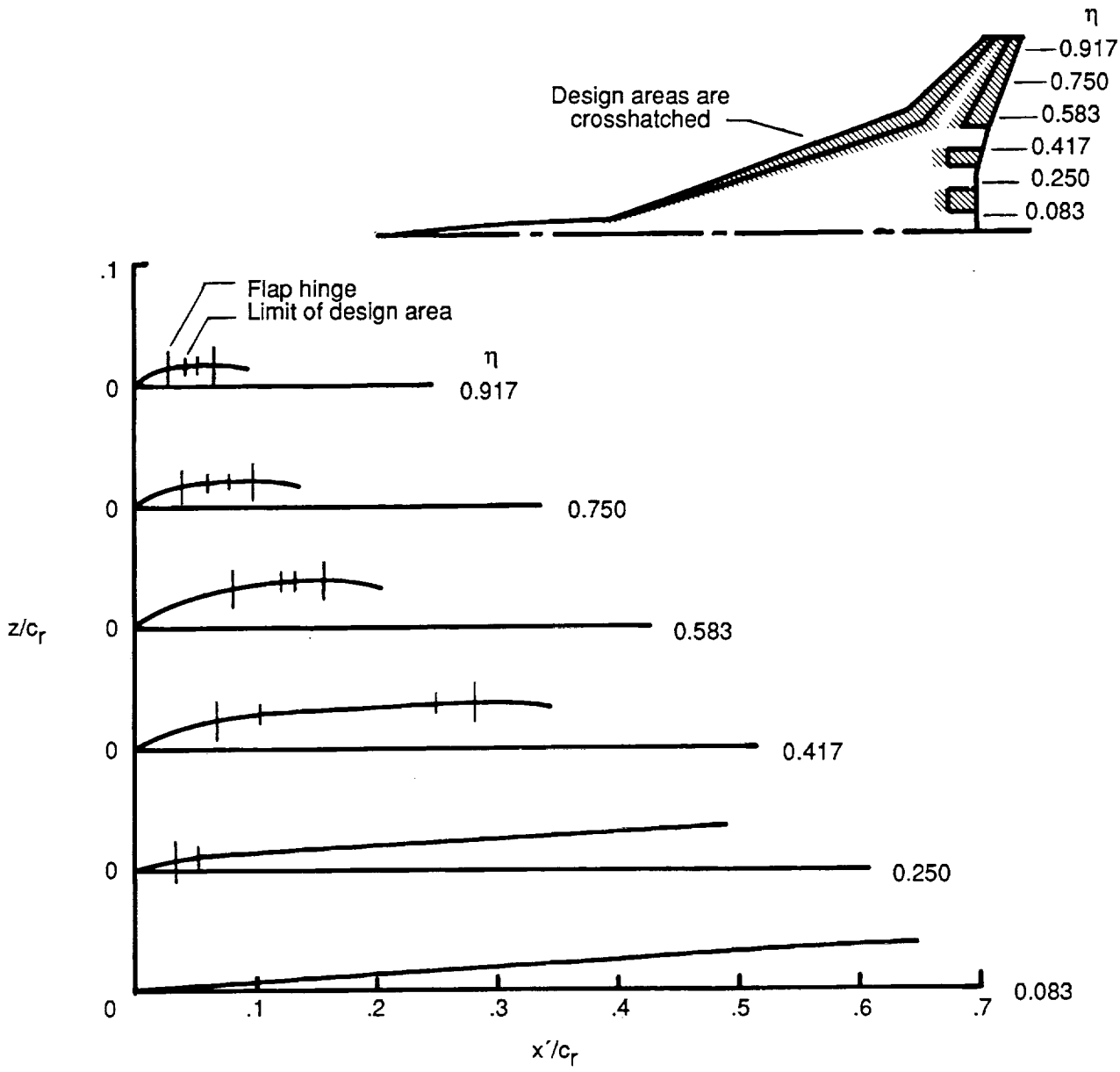

Figure 7. Camber surface of restricted-area design used in definition of baseline flap system. $c_{f,\mathrm{le},o} = 0.30c$; $c_{f,\mathrm{le,sf}} = 0$; $M = 0.20$; $C_{L,\mathrm{des}} = 0.45$; $C_{m,\mathrm{des}} = -0.03$. Camber surface shown at $\alpha = -3.2°$.

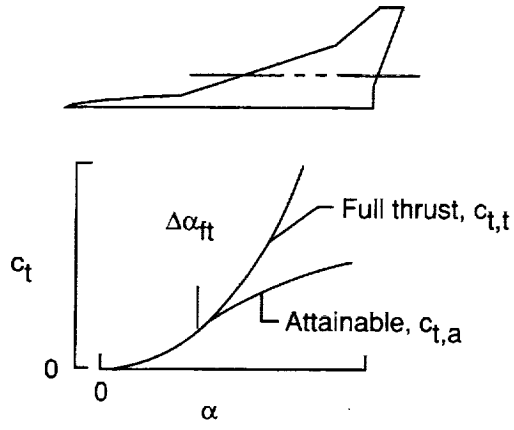

(a) Leading-edge thrust of flat-wing section.

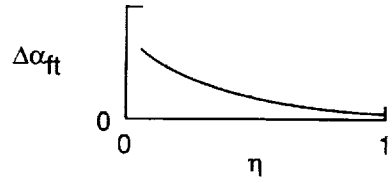

(b) Angle-of-attack range for full leading-edge thrust.

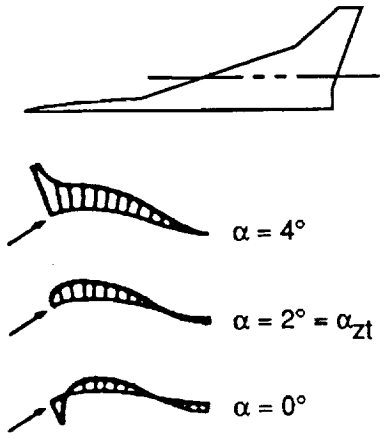

(c) Definition of angle of attack for zero leading-edge thrust at given span station.

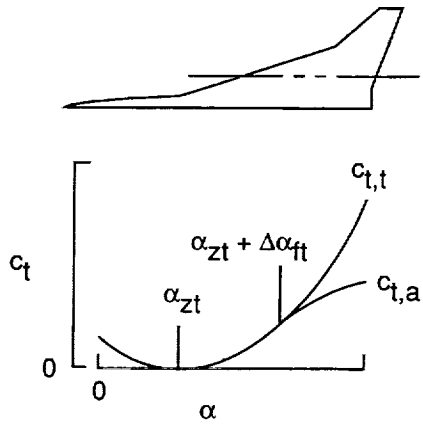

(d) Leading-edge thrust of twisted and cambered wing section.

Figure 8. Leading-edge thrust characteristics of wing section.

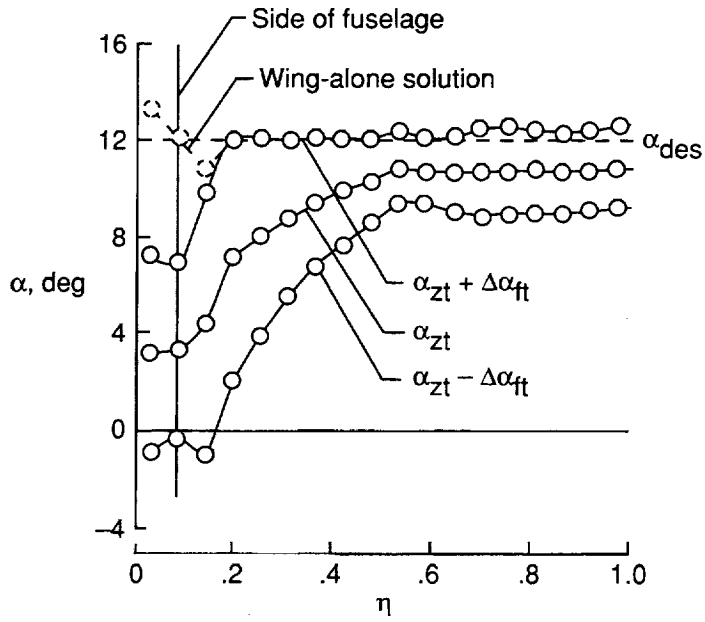

Figure 9. Range of full leading-edge thrust from WINGDES2 code for restricted-area camber surface design for baseline case. $c_{f,\mathrm{le},o} = 0.30c$; $c_{f,\mathrm{le,sf}} = 0$; $M = 0.20$; $C_{L,\mathrm{des}} = 0.45$; $C_{m,\mathrm{des}} = -0.03$.

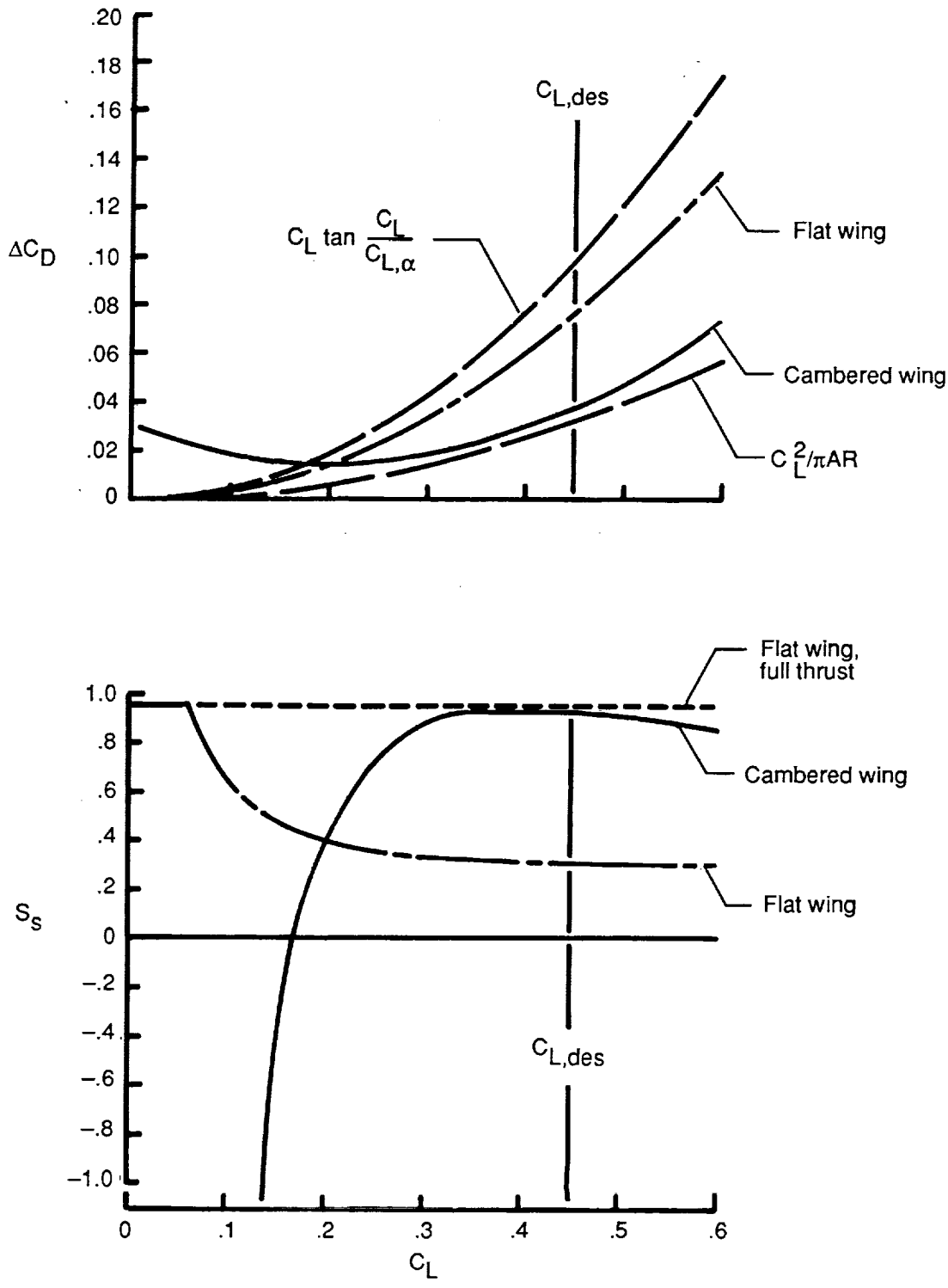

Figure 10. Performance of restricted-area camber surface design for baseline case. $c_{f,\mathrm{le},o} = 0.30c$; $c_{f,\mathrm{le,sf}} = 0$; $M = 0.20$; $C_{L,\mathrm{des}} = 0.45$; $C_{m,\mathrm{des}} = -0.03$.

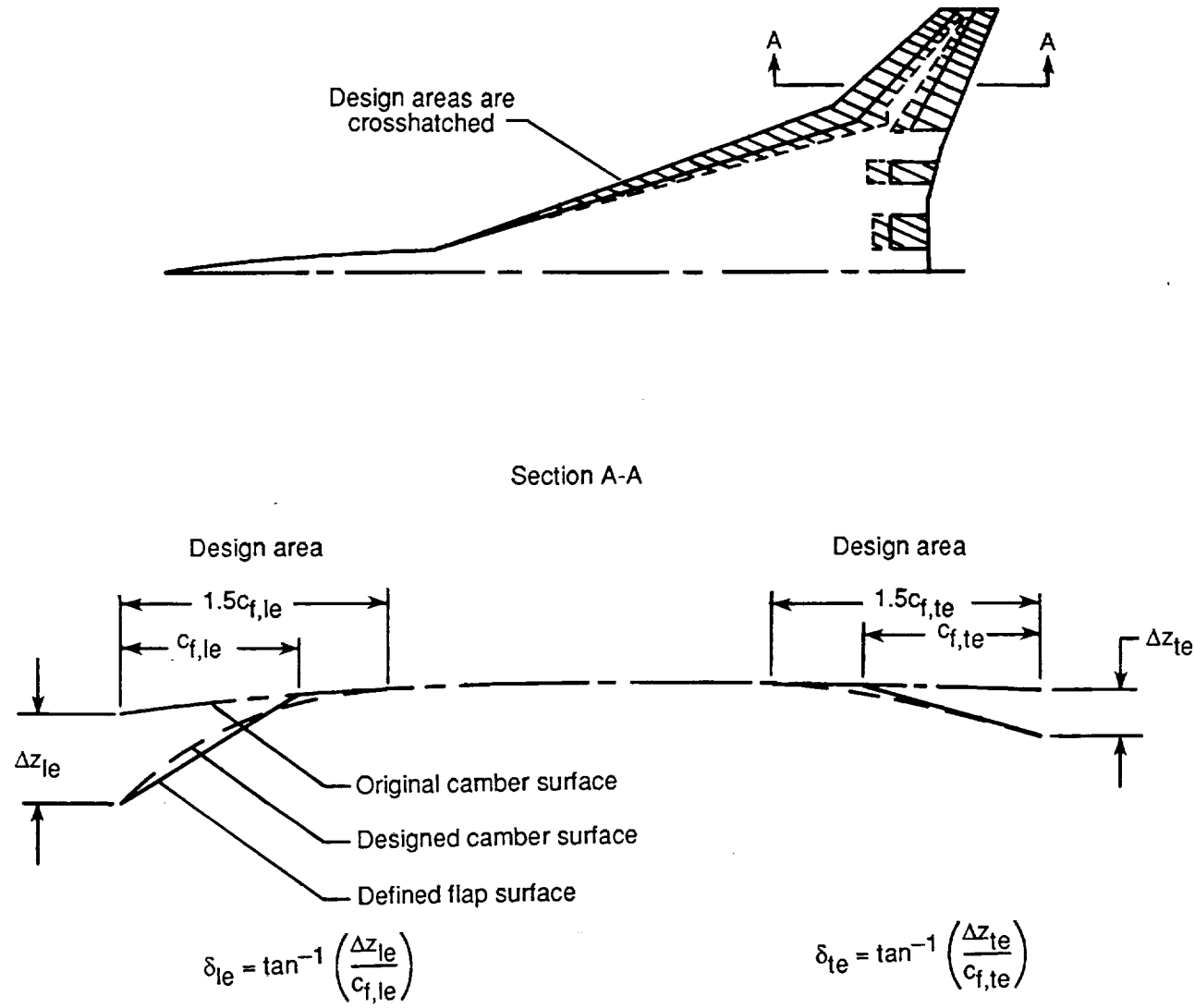

Figure 11. Determination of flat-wing flap-deflection angles that approximate camber surface of restricted-area designs.

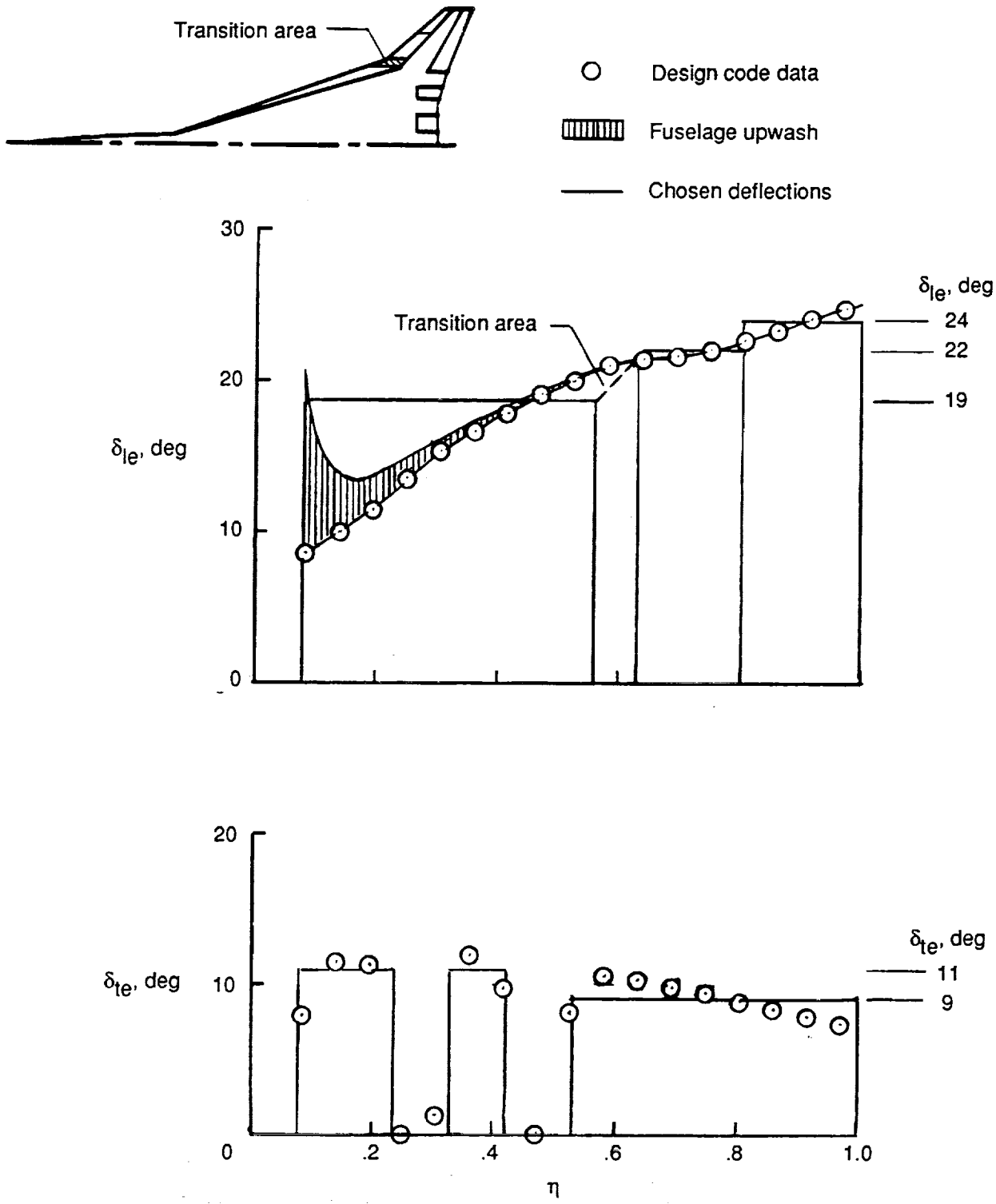

Figure 12. Spanwise flap-deflection schedule approximating restricted-area camber surface design for baseline case. $c_{f,\mathrm{le},o} = 0.30c$; $c_{f,\mathrm{le,sf}} = 0$; $M = 0.20$; $C_{L,\mathrm{des}} = 0.45$; $C_{m,\mathrm{des}} = -0.03$.

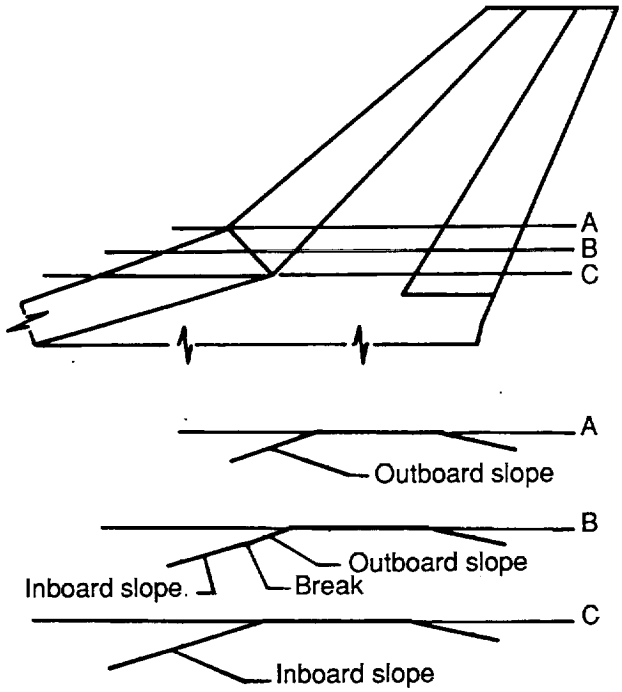

Figure 13. Possible treatment of inboard and outboard flap connections to minimize flow separation.

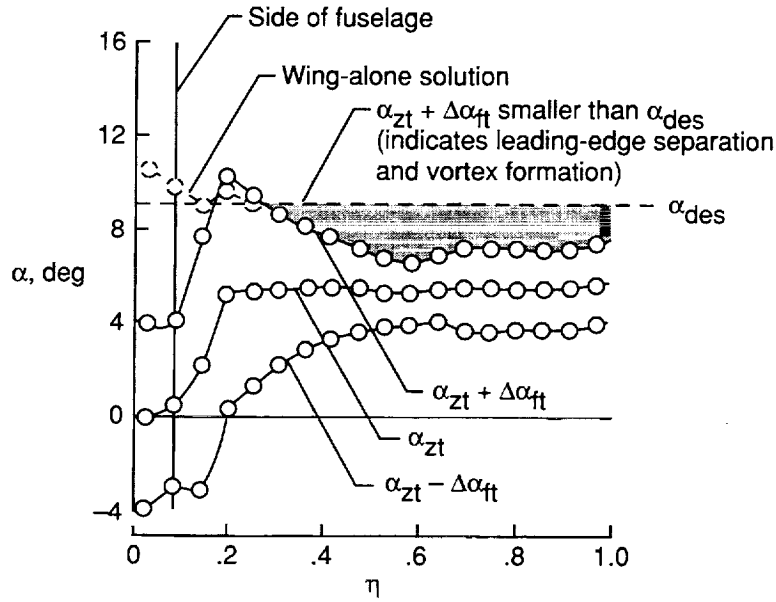

Figure 14. Range of full leading-edge thrust from AERO2S code for wing with flaps deflected to approximate restricted-area camber surface design for baseline case ($\delta_{le} = 19°/22°/24°$, $\delta_{te} = 11°/9°$). $c_{f,le,o} = 0.30c$; $c_{f,le,sf} = 0$; $M = 0.20$; $C_{L,des} = 0.45$; $C_{m,des} = -0.03$.

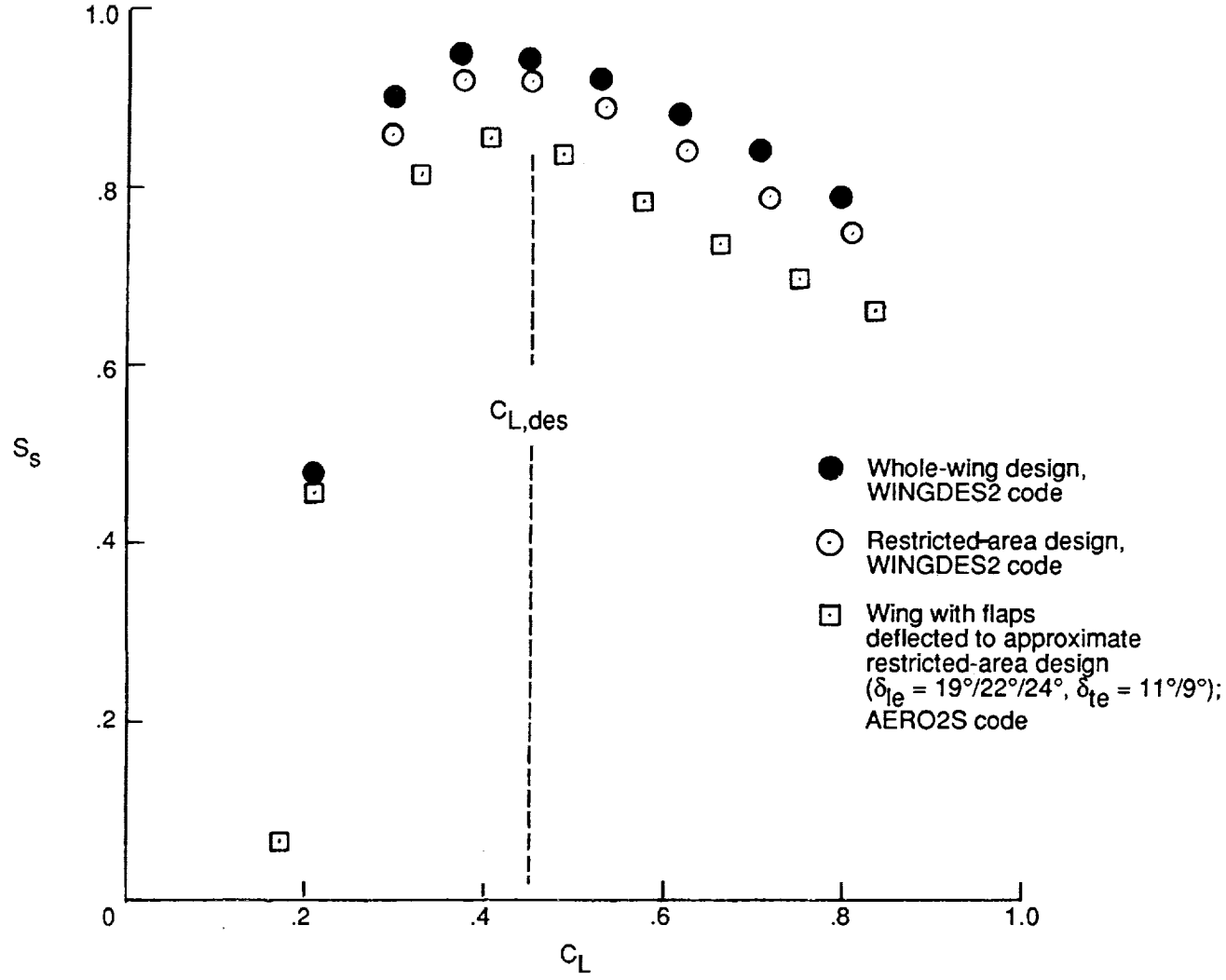

Figure 15. Performance of baseline flap system compared with cambered-wing designs used in its derivation. $M = 0.20$; $C_{L,\text{des}} = 0.45$. Restricted-area design: $C_{m,\text{des}} = -0.03$. Flaps and restricted-area design: $c_{f,\text{le},o} = 0.30c$, $c_{f,\text{le,sf}} = 0$.

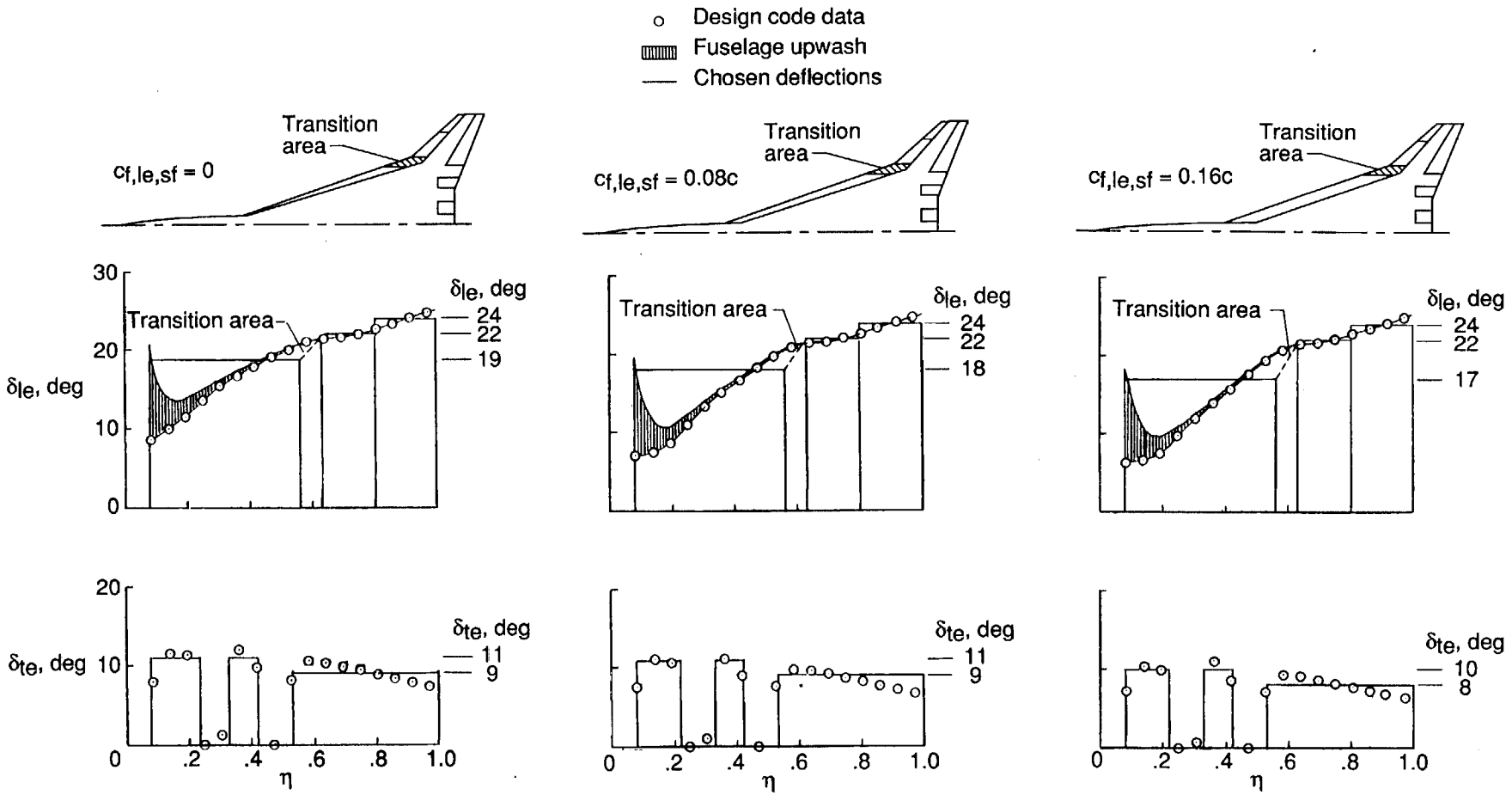

(a) Variation of inboard leading-edge flap chord; $c_{f,\mathrm{le},o} = 0.30c$.

Figure 16. Spanwise flap-deflection schedules approximating restricted-area camber surface design for various flap systems. $M = 0.20$; $C_{L,\mathrm{des}} = 0.45$; $C_{m,\mathrm{des}} = -0.03$.

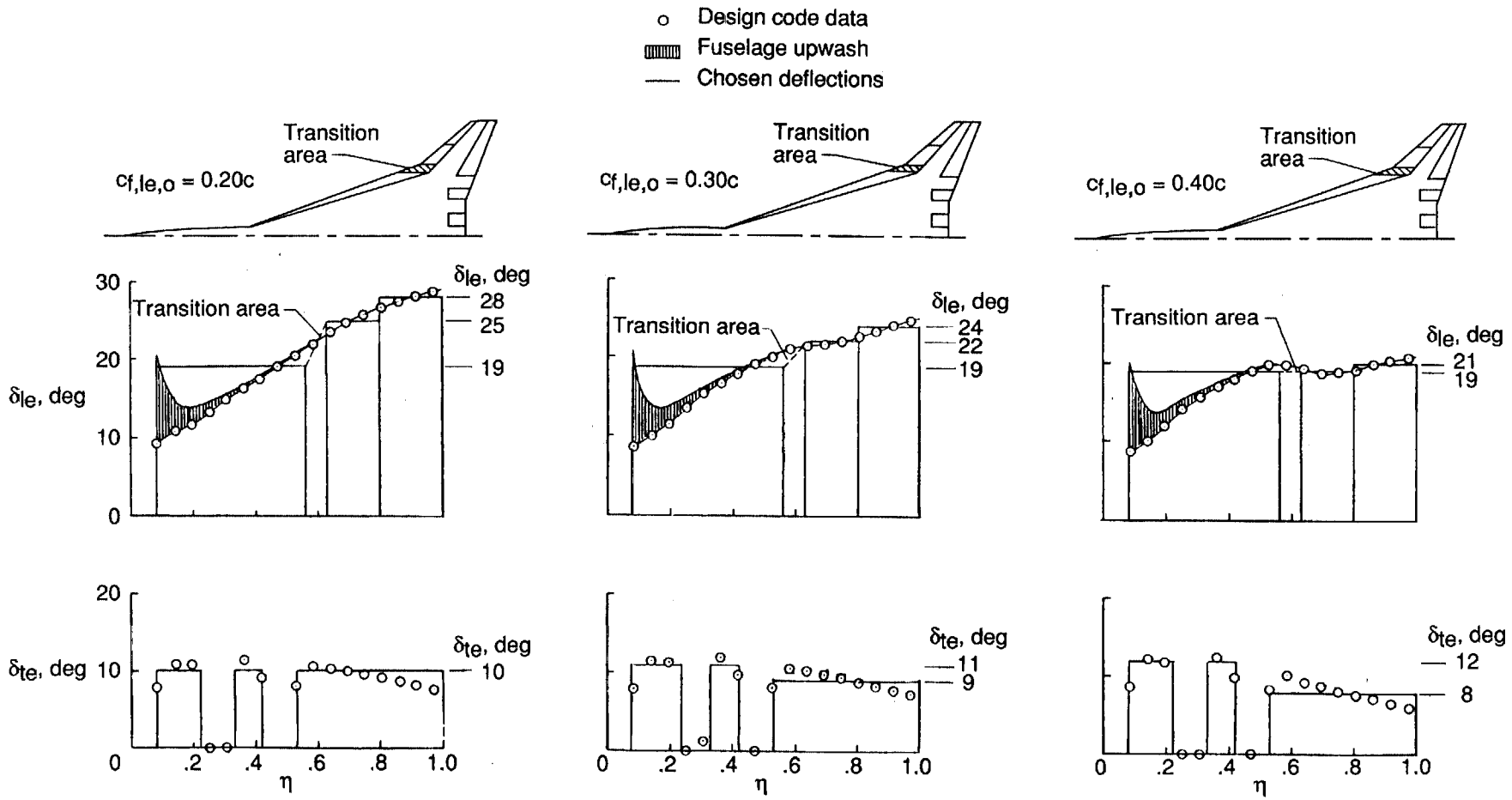

(b) Variation of outboard leading-edge flap chord; $c_{f,\mathrm{le,sf}} = 0$.

Figure 16. Concluded.

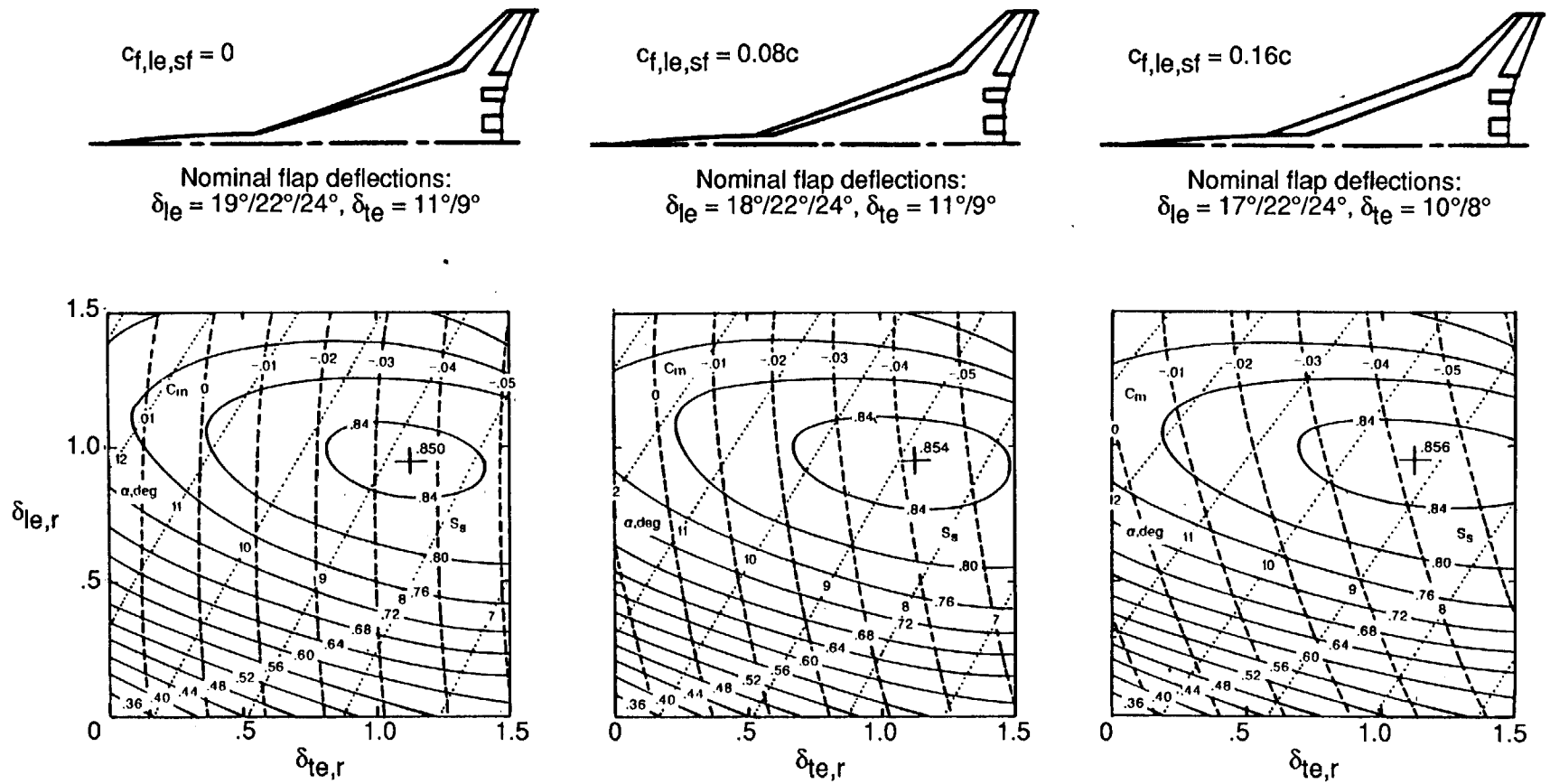

(a) Variation of inboard leading-edge flap chord; $c_{f,\mathrm{le},o} = 0.30c$.

Figure 17. Performance contour maps for various flap systems illustrating effect of departures from nominal flap deflections shown in figure 16. $M = 0.20$; $C_L = 0.45$.

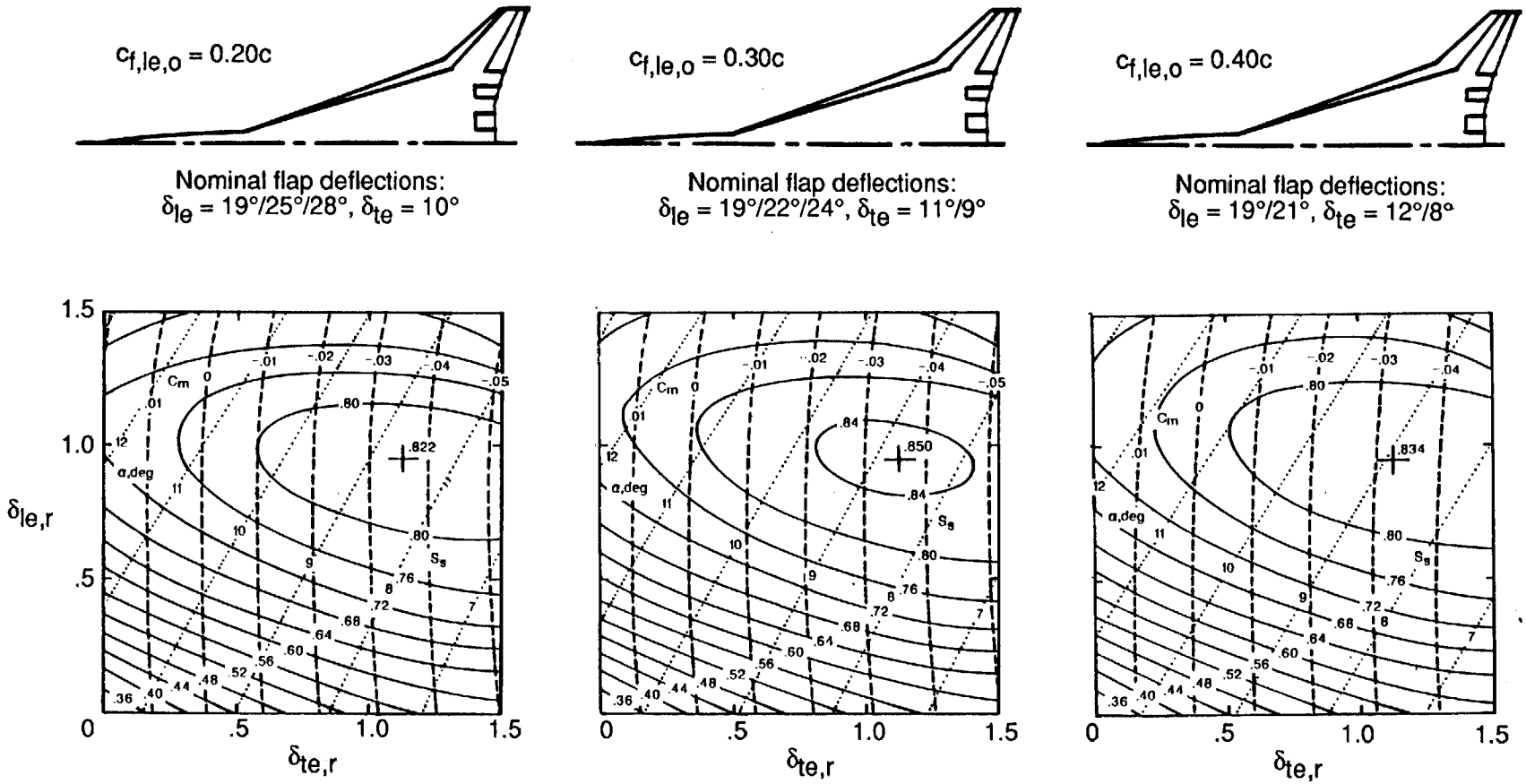

(b) Variation of outboard leading-edge flap chord; $c_{f,le,sf} = 0$.

Figure 17. Concluded.

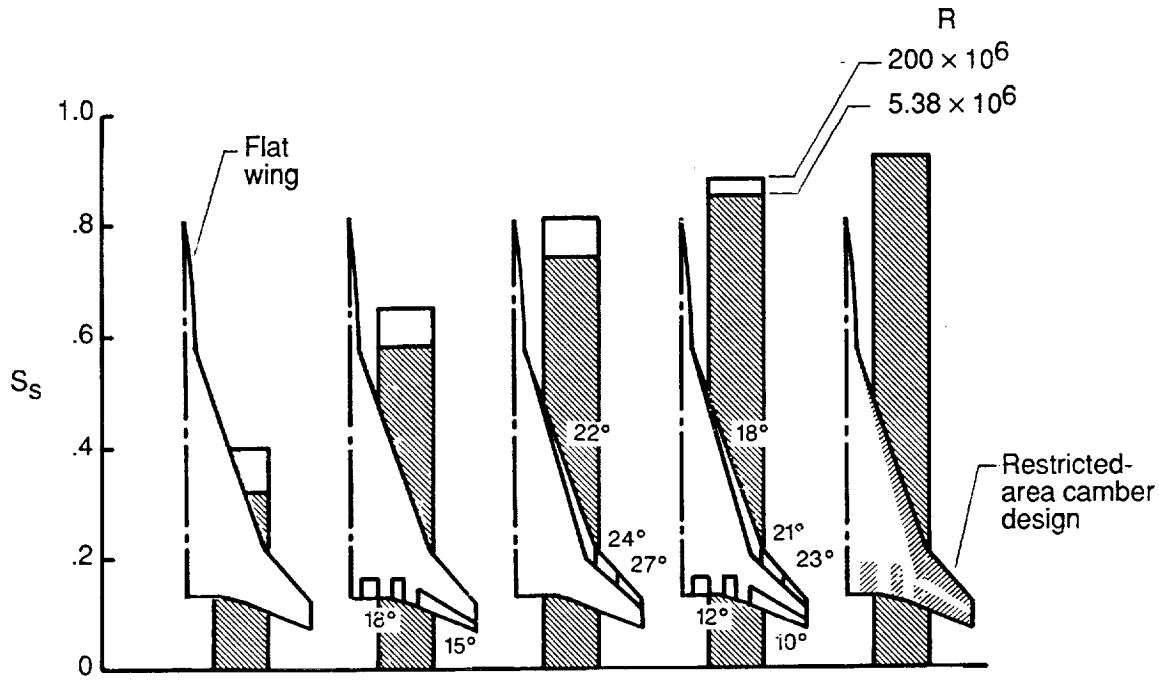

Figure 18. Flap-system performance compared with that of flat wing and restricted-area camber surface design from which it was derived. Optimized deflections are given for $M = 0.20$ and $C_L = 0.45$. Baseline flap geometry; flap deflections are given adjacent to each flap.

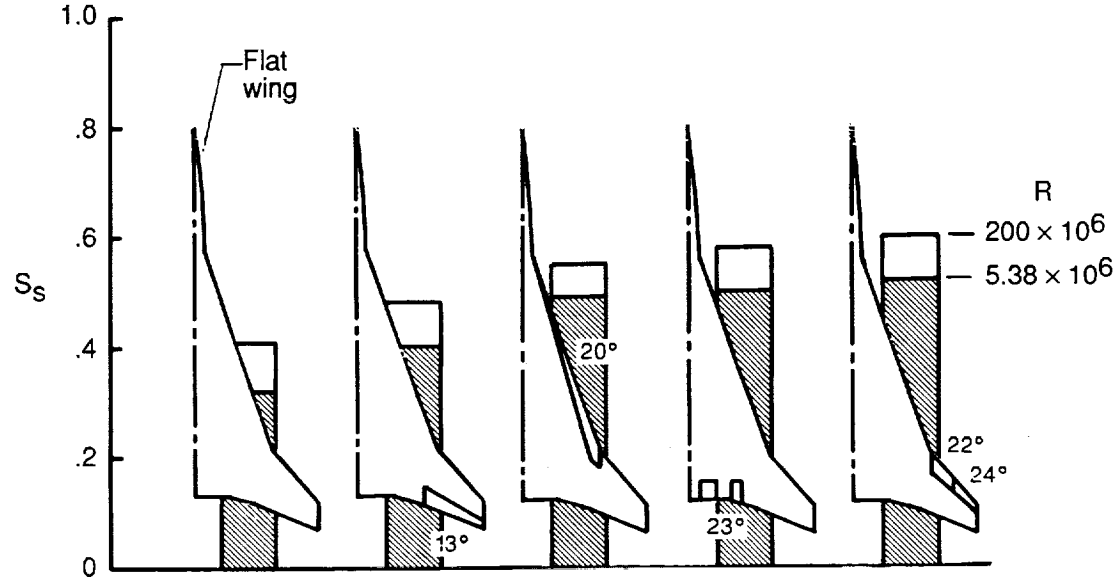

Figure 19. Performance of individual leading- and trailing-edge flaps with optimized deflections for $M = 0.20$ and $C_L = 0.45$. Baseline flap geometry; flap deflections are given adjacent to each flap.

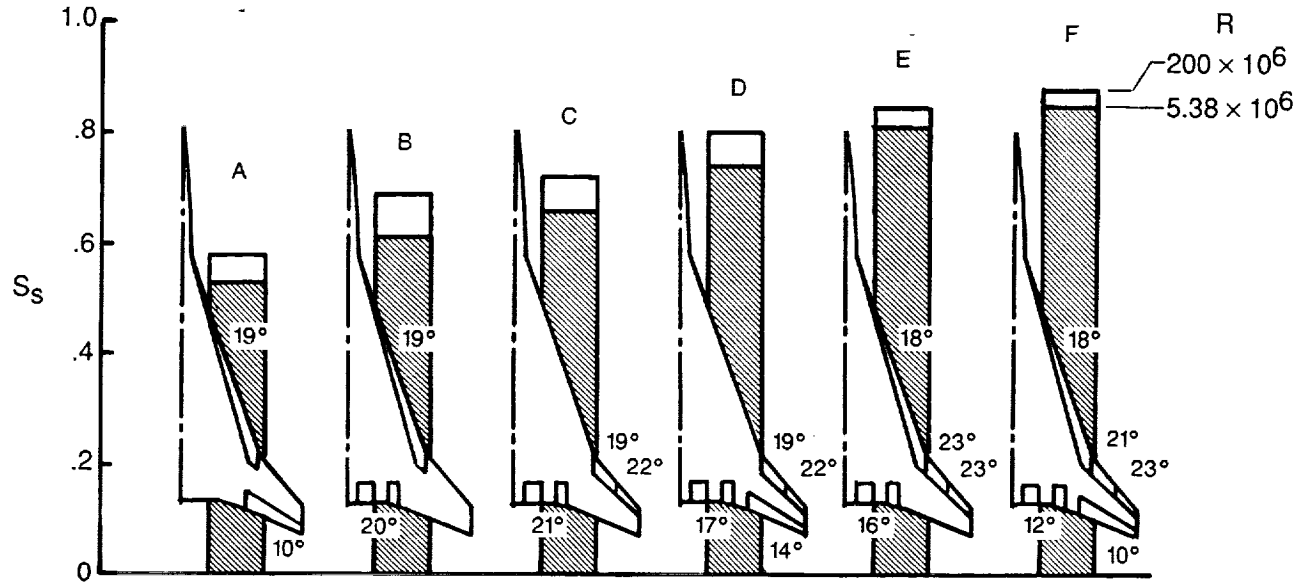

(a) No moment restraint.

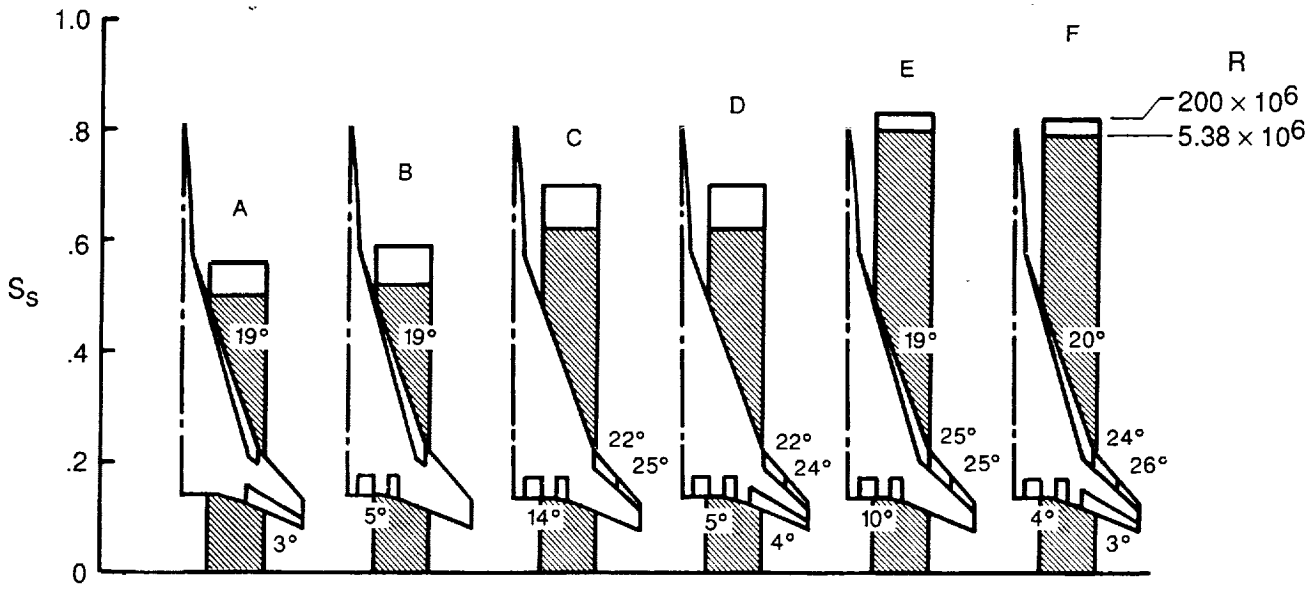

(b) With zero pitching-moment restraint.

Figure 20. Performance of various combinations of leading- and trailing-edge flaps with optimized deflections for $M = 0.20$ and $C_L = 0.45$. Baseline flap geometry; flap deflections are given adjacent to each flap.

REPORT DOCUMENTATION PAGE

Form Approved
OMB No. 0704-0188

1. AGENCY USE ONLY *(Leave blank)*	2. REPORT DATE	3. REPORT TYPE AND DATES COVERED
	December 1999	Technical Publication

4. TITLE AND SUBTITLE
Design of Supersonic Transport Flap Systems for Thrust Recovery at Subsonic Speeds

5. FUNDING NUMBERS
WU 537-09-20-02

6. AUTHOR(S)
Michael J. Mann, Harry W. Carlson, and Christopher S. Domack

7. PERFORMING ORGANIZATION NAME(S) AND ADDRESS(ES)
NASA Langley Research Center
Hampton, VA 23681-2199

8. PERFORMING ORGANIZATION REPORT NUMBER
L-17279

9. SPONSORING/MONITORING AGENCY NAME(S) AND ADDRESS(ES)
National Aeronautics and Space Administration
Washington, DC 20546-0001

10. SPONSORING/MONITORING AGENCY REPORT NUMBER
NASA/TP-1999-209536

11. SUPPLEMENTARY NOTES
Mann: Langley Research Center, Hampton, VA; Carlson and Domack: Lockheed Engineering & Sciences Company, Hampton, VA.

12a. DISTRIBUTION/AVAILABILITY STATEMENT
Unclassified–Unlimited
Subject Category 05 Distribution: Nonstandard
Availability: NASA CASI (301) 621-0390

12b. DISTRIBUTION CODE

13. ABSTRACT *(Maximum 200 words)*

A study of the subsonic aerodynamics of hinged flap systems for supersonic cruise commercial aircraft has been conducted using linear attached-flow theory that has been modified to include an estimate of attainable leading-edge thrust and an approximate representation of vortex forces. Comparisons of theoretical predictions with experimental results show that the theory gives a reasonably good and generally conservative estimate of the performance of an efficient flap system and provides a good estimate of the leading- and trailing-edge deflection angles necessary for optimum performance. A substantial reduction in the area of the inboard region of the leading-edge flap has only a minor effect on the performance and the optimum deflection angles. Changes in the size of the outboard leading-edge flap show that performance is greatest when this flap has a chord equal to approximately 30 percent of the wing chord. A study was also made of the performance of various combinations of individual leading- and trailing-edge flaps, and the results show that aerodynamic efficiences as high as 85 percent of full suction are predicted.

14. SUBJECT TERMS	15. NUMBER OF PAGES
Flap systems; Supersonic transport; High-speed civil transport; Linear theory	51
	16. PRICE CODE: A04

17. SECURITY CLASSIFICATION OF REPORT	18. SECURITY CLASSIFICATION OF THIS PAGE	19. SECURITY CLASSIFICATION OF ABSTRACT	20. LIMITATION OF ABSTRACT
Unclassified	Unclassified	Unclassified	UL